ETH
Eidgenössische Technische Hochschule Zürich
Swiss Federal Institute of Technology Zurich

Reaction-diffusion models in the context of brain tumours

Bachelor Thesis

Julius Michael Maximilian Siebenaller

Tuesday 25th June, 2024

Advisor: Dr. Laura Gioia Andrea Kobel-Keller

Department of Mathematics, ETH Zürich

Abstract

Gliomas form the majority of primary brain tumours and possess a plethora of mechanisms that constitute their malignant potential. One of these mechanisms concerns the ability to adjust their phenotype to the respective environment such that they either proliferate or migrate. The migration-proliferation dichotomy can be modelled in a system of partial differential equations, describing the interplay of glioma cell density, oxygen concentration and the density of functional tumour vasculature. This thesis discusses parts of the Alfonso et al. model. We provide a brief overview of the biology of cancer and especially of gliomas to give a basic understanding. Additionally, we embed the model in the theory of PDEs, in particular the theory of reaction-diffusion equations, giving a theoretical overview, analysing the Fisher-Kolmogoroff equation and explaining the origin of reaction-diffusion systems. This thesis finishes by discussing the simulation results of the model and by providing an outlook for subsequent works. This model confirms the migration-dichotomy of glioma cells. We find that mainly the diffusion and proliferation rates describe the malignant potential of glioma cells. The vaso-occlusion rate shows only a small influence, but an increase in the oxygen consumption rate limits the tumour growth.

Contents

Chapter 1

Introduction

The World Health Organisation [33, 43] classifies tumours according to their prospective clinical outcomes. Regarding brain tumours, all of them showcase infiltrative properties and most of them are classified as malignant. Gliomas are found to be the most abundant occurring type of primary brain tumours and showcase certain abnormalities that serve as defence mechanism and increase their malignant potential (c.f. Ahir et al. [3], Giaume et al. [15], Götz [19], Lassman [32], Rasmussen [48] or Westphal and Lamszus [53]).

Following Böttger et al. [7, 8], Gao et al. [14] or Pham et al. [47], one of these mechanisms concerns the migration-proliferation dichotomy. Glioma cells feature both a migratory and a proliferatory behaviour depending on their phenotype. They can switch their phenotype to adapt to the respective environment.

The migration-proliferation dichotomy is yet to be fully understood, but mathematical models have provided immense value along the way. Bull and Byrne [6] and Kuznetsov et al. [30] provide an overview of modelling approaches used in mathematical oncology. Next to using ordinary differential equations, or agent-based models, relying on partial differential equations has been shown to be a powerful tool to describe behaviours of cancer cells. Alfonso et al. [5], Pham et al. [47] or Swanson et al. [50] utilise systems of reaction-diffusion PDEs to model the migration-proliferation dichotomy of glioma cells.

The model of Alfonso et al. [5] describes the behaviour of glioma cells in the brain. They focus on the interplay of glioma cell density, oxygen concentration and density of functional tumour vasculature to describe the migration-proliferation dichotomy of glioma cells. We replicate the model and analyse different cases, varying the main parameters. These include the glioma cell diffusion and proliferation rates, as well as the oxygen consumption rate of gliomas and the vaso-occlusion rate. We find that an increase in the diffusion

and the proliferation rates provides the most distinct effects. For higher rates, the tumour shows a more malignant behaviour, spreading farther into the brain and growing stronger at each site. We also find that increasing the oxygen consumption rate significantly limits the proliferation of the tumour. The growth is restricted since the brain tissue becomes oxygen depleted at a faster rate. Increasing the vaso-occlusion rate does not provide significant changes regarding the malignancy of the tumour. But we see a more distinct vaso-occlusion, especially in the case of higher diffusion and proliferation rates. We confirm the migration-dichotomy of glioma cells in this model.

In this thesis, we focus on reaction-diffusion models in the context of brain tumours, analysing the migration-proliferation model of Alfonso et al. [5]. In chapter 2, we provide a short overview regarding the biology of tumours and gliomas. We explain the hallmarks of cancer to provide a basic understanding and give an overview of the properties of gliomas. In particular, we describe behaviour, function, and structure of gliomas, which cause them to resist treatment and lead to their increased survival and growth rates. We finish this chapter by outlining the model assumptions for the Alfonso et al. [5] migration-proliferation model. Chapter 3 provides a theoretical overview regarding reaction-diffusion equations. We analyse the particular example of the Fisher-Kolmogoroff equation and explain that balance laws form the basis for reaction-diffusion systems. This chapter finishes by showing how the diffusion equation can be derived from a simple random walk approach. Chapter 4 describes the migration-proliferation dichotomy model following the work of Alfonso et al. [5]. We replicate the model and provide a numerical analysis for varying parameters. Chapter 5 concludes this thesis by discussing the results and by providing an outlook for future works.

Chapter 2

Biology of Tumours and Gliomas

Cancer, and in particular the development of tumours in humans, can be described along six, respectively now ten, hallmarks and characteristics. These are described in the seminal works of Hanahan and Weinberg [21, 22] and further extended by Hanahan [20]. Here, we present these hallmarks and then provide a brief explanation of the biology of glioma cells. In particular, this should provide a solid background to understand the assumptions taken in the model of Alfonso et al. [5]. Given the scope of this thesis, only a brief overview of the involved biology can be provided and the reader is referred to the chosen literature for a more detailed understanding.

2.1 The Hallmarks of Cancer

Hanahan and Weinberg [21, 22] and then extended by Hanahan [20], categorise cancer along the following hallmarks:

1. **Sustaining proliferative signaling** (Originally: Self-sufficiency in growth signals): Compared to normal cells, tumour cells are less reliant on growth signals for proliferation and even generate growth signals autonomously. The loss and absence of control mechanisms and further the ability to sustain proliferation by chronically sending proliferative signals via a plethora of ways, shows that tumour cells behave abnormally.
2. **Evading growth suppressors** (Originally: Insensitivity to antigrowth signals): Cell proliferation is suppressed by anti-growth signals that are forcing cells into a quiescent state. These signals are often mediated by the retinoblastoma protein (pRb) and tumours sustain proliferation by blocking or altering this path.
3. **Resisting cell death** (Originally: Evading apoptosis): Tumour cells resist programmed cell death, termed apoptosis, via sensors and effec-

tors. Sensors survey the cell environment and send according signals to cells, thus regulating effectors of apoptotic death. For example, cell surface receptors recognize survival and death signals from ligands and receptors that originate from the surrounding cells or from the cells themselves.

4. **Enabling replicative immortality** (Originally: Limitless replicative potential): Cells are found to possess an intrinsic regulatory mechanism limiting the cell proliferation. The term senescence describes the phenomenon of cells ending the iteration process after a certain number of iterations. Tumour cells evade senescence by blocking suppressor proteins (pRb and p53) until a so-called crisis state is reached. In this state, immortalization, the limitless multiplication of cells as observed in culture, is a key feature of tumour cells and promotes tumour growth.
5. **Inducing angiogenesis** (Originally: Sustained angiogenesis): Oxygen and nutrients are critical for the survival and functioning of cells. Both are provided by the vasculature. But normal cells are observed to have only a limited capacity of angiogenesis. So they can only form new vasculature in a restricted manner, which limits their growth potential and ensures tissue structure. On the other hand, tumour cells can induce and further sustain angiogenesis via a plethora of mechanisms, inducing the release of different growth factors that promote angiogenesis.
6. **Activating invasion and metastatsis** (Originally: Tissue Invasion and Metastasis): Tumour cells invade their neighbourhood and proliferate away from the original side. This allows the tumour to sustain growth by spreading into new regions, hence accessing further resources to fuel the tumour growth.

The original six hallmarks are further extended to include two enabling characteristics (cf. Hanahan and Weinberg [20, 22]):

7. **Genome instability and mutation**: Tumour cells progress and tumours expand by generating clones that can survive and succeed in the given environment. The ability to alter the genome in the process of clonal expansions is based on an increased rate of mutation. This increase in the rate of mutation itself occurs via an increased sensitivity to mutagenic agents and the ability to circumvent surveillance systems. These mechanisms show key characteristics of tumour cells.
8. **Tumour-promoting inflammation**: Tumour cells possess the special ability to, at least to some extent, utilise inflammation, thus circumventing a particular defence mechanism of the immune system. In fact, inflammation can contribute in parts to all the above hallmarks.

And to include two emerging hallmarks:

9. **Reprogramming Energy Metabolism**: Tumour cells are shown to be able to adjust the energy metabolism to fit the given environment. Whereas normal cells process glucose in aerobic conditions and rely on glycolysis given an anaerobic environment, tumour cells are shown to be able to adjust the metabolism and also rely on glycolysis in aerobic conditions, giving them an additional edge for their survival. In principle, all cells can adjust their energy metabolism to some extent, but tumours are special since they can maintain a highly proliferative state even in the absence of sufficient amounts of oxygen.
10. **Evading Immune Destruction**: Immune surveillance provides a critical defence mechanism against the tumourigenesis and the progression of tumours. Nonetheless, tumour cells can survive and proliferate by being able to avoid detection and disabling other defence mechanisms of the immune system.

Hanahan further adds [20]:

11. **Unlocking phenotypic plasticity**
12. **Nonmutational epigenetic reprogramming**
13. **Polymorphic microbiomes**
14. **Senescent cells**

to the list of emerging hallmarks and enabling characteristics. This provides us with an overview of key features of tumour cells. We further explain these features in the following section to provide additional details regarding the migration-proliferation dichotomy of glioma cells.

2.2 Properties of gliomas

The interest in studying gliomas arises not only due to their specific properties, but also since they are found to be the most abundant occurring type of primary brain tumours. Gliomas arise from glial cells in the central nervous system and diffuse mainly in the brain, so their occurrence is locally restricted. Glial cells themselves are critical for the functioning of the central nervous system, serve as protectors and help repair damages to the brain (cf. Giaume et al. [15], Götz [19], and Jessen [28]). The connection of gliomas to a crucial part of the central nervous system underlines the interest in studying these tumours (cf. Ahir et al. [3], Lassmann [32], Rasmussen [48], Westphal and Lamszus [53]).

On a general basis, the World Health Organisation classifies tumours according to their prospective clinical outcomes and provides six different groups to classify tumours of the central nervous system. Amongst adult-type diffuse gliomas, we have astrocytomas, oligodendrogliomas and glioblastomas. The

respective grading ranges from grade 2 to grade 4 for astrocytomas, from grade 2 to grade 3 for oligodendrogliomas and grade 4 is assigned to glioblastomas. Compared to grade 1 tumours, which are characterised by having only a low proliferative profile, tumours of grade 2 and higher showcase infiltrative properties. Gliomas are all characterised by infiltrative behaviour and we are often dealing with malignant cases and fatal outcomes for grade 4 astrocytomas and glioblastomas (cf. WHO Classification of Tumours of the Central Nervous System [33, 43]).

Glioma cells showcase certain abnormalities in terms of their behaviour, their function, and on a structural level, that cause them to resist treatment and lead to their increased survival and growth rates. In the following, we highlight the migration-proliferation dichotomy and the process of tumour angiogenesis.

Gliomas feature both a migratory and a proliferatory behaviour depending on their phenotype, which is shown in the work of Gao et al. [14]. The pathways which activate the migration or proliferation behaviours cooperate in the cells. Moreover, glioma cells are able to switch their phenotype to adapt and survive in the respective environment. In hypoxic environments, which are characterised by low oxygen levels, tumour cells migrate to access resources provided by a different environment. Whereas in normoxic environments, characterised by normal oxygen levels, tumour cells have a proliferative phenotype. The oxygen level in normal brain tissue, is roughly 3.5%, so about 26mmHg. An environment with oxygen levels lower than 2% can be considered hypoxic. In the model of Alfonso et al. [5], a threshold for hypoxia is assumed to be at 10mmHg. This ability to switch phenotypes is a critical factor that supports tumour survival and growth of glioma cells (cf. Alfonso et al. [5], Böttger et al. [7], Böttger et al. [8], Gao et al. [14], Giese et al. [16], McKeown [39] and Pham et al. [47]).

Cell proliferation relies indirectly on angiogenesis. Jain et al. [26] describe angiogenesis as the process of new blood vessel formation, by endothelial cells, from pre-existing adjacent vessels. As outlined in Carmeliet and Jain [10] and Lugano et al. [34], cells rely on the blood circulation system to provide resources in form of oxygen and nutrients. Therefore, being in close range to blood vessels is critical for survival. In contrast to normal cells, tumour cells showcase different angiogenetic processes to guarantee their survival and growth. Ahir et al. [3] and Carmeliet and Jain [10] describe that angiogenesis is controlled by pro- and anti-angiogenetic factors. Given the structure of tumour cells, the production rate of pro-angiogenic factors is very high. Tumour cells demonstrate an abnormal structure, since branching and growth of the vessel network follows an unpredictable and irregular course. Additionally, tumour vessels are heterogeneous in terms of having various sub-types and different diameters.

Jain et al. [26] and Lugano et al. [34] further explain that due to this heterogeneity, the function of tumour vessels is compromised, which leads to an environment characterised by hypoxia, by a low availability of nutrients and by a high interstitial fluid pressure. In this hostile environment, tumour cells release more pro-angiogenic factors to grow new vessels to access the blood system. This results in a destructive cycle as the tumour grows while the surrounding environment remains hostile. In this environment an evolution-like process occurs, resulting in the selection of malignant phenotypes that are more suited for survival. As outlined above, and also presented in Carmeliet and Jain [10], the blood flow is further disrupted by the migration behaviour, which allows the cells to spread to less hostile environments. Here, angiogenesis and the environment play mediating roles for the switching of phenotypes (cf. Giese et al. [16]).

Last but not least, the proliferation of tumour cells induces another mechanism that further contributes to the malignancy of cancer cells as is explained in the works of Giese et al. [16], Jain et al. [27] and Padera et al. [46]. Tumour invasion and growth is in part due to an increase in the structural components, i.e. the number and size of cells. Given this rise in tumour size and number, adjacent tissues are displaced, which provides further space for tumour invasion and growth. The involved mechanical forces adversely affect the tumour and the environment via both solid and fluid stress. This leads to a compression of blood and lymphatic vessels and lower tumour perfusion rates. Since the supply system of nutrients and oxygen is restricted, the environment is characterised by low oxygen level but high acidity. Also, a high density of tumour cells has another negative effect on the surrounding environment, since the exerted pressure leads to collapse of adjacent vessels and impaired functions of tumour vessels. This contributes further to the vicious cycle as outlined above. For more insights into the role of mechanic properties of cancer cells on their growth and progression, the interested reader is referred to the works of Ahmed et al. [4], Follain et al. [13], Macnamara [35] and Massey et al. [38].

2.3 Model Assumptions

The model in Alfonso et al. [5] describes the feedback mechanisms between glioma cells and the brain vasculature. Of particular interest are the proliferation-migration dichotomy, the vaso-occlusion at the tissue borders and the interaction of these factors. We state the assumptions in the model and provide a brief explanation of the underlying biological mechanisms. The mathematical model itself will be explained in chapter 4.

Their approach is based on the following assumptions [5]:

1. In a normoxic environment, characterised by normal oxygen levels,

glioma cells have a proliferative phenotype, whereas in a hypoxic environment, characterised by low levels of oxygen, the phenoytpe is migratory. Glioma cells switch phenotypes to adapt to the respective environment.

2. Glioma cells excrete pro-angiogenic factors in hypoxic conditions.
3. Regulation of vasculature remodelling and the formation of blood vessels are induced by pro-angiogenic factors.
4. Pro-angiogenic factors are absorbed by endothelial cells. These cells form the vacscular network.
5. Oxygen is released by functional tumour blood vessels.
6. Oxygen is a key factor for the growth and progression of gliomas.
7. Oxygen, provided by a functional vasculature, is consumed by glioma cells.
8. Blood vessel occlusion and collapse are promoted by prothrombotic factors and increased mechanical pressure in regions that are characterised by high density of glioma cells.

Comparing the model assumptions with the hallmarks of cancer in section 2.1, especially (1) sustaining proliferative signaling, (5) inducing angiogenesis, (6) activating invasion and metastasis (9) reprogramming energy matabolism and (11) unlocking phenotypic plasticity, are reflected in the work of Alfonso et al. [5].

Chapter 3

On Reaction-Diffusion Systems

This chapter provides a short introduction to reaction-diffusion systems. At first, we describe diffusion and reaction-diffusion equations and their foundation in general balance laws. Then, we derive the diffusion equation following a simple random walk approach to provide some more details. The Fisher-Kolmogoroff Equation serves as a particular example for a nonlinear reaction-diffusion equation and we analyse the steady states and travelling wave solutions of this equation.

3.1 Diffusion and Reaction-Diffusion Equations

As is shown in the works of Evans [11] and Grindrod [18], a simple case of a *diffusion equation* is given as

$$\frac{\partial u}{\partial t} = \Delta u, \tag{3.1}$$

for $u : \Omega \subseteq \mathbb{R}^n \times \mathbb{R}_{>0} \to \mathbb{R}$, $\Omega \subset \mathbb{R}^n$ open, representing the density of a given entity at a point $x \in \Omega$ in space at time $t \in \mathbb{R}$. Equation (3.1) represents a linear partial differential equation. In the nonhomogeneous case, we modify equation (3.1) and obtain a more general version of the *diffusion equation*:

$$\frac{\partial u}{\partial t} - \Delta u = f, \tag{3.2}$$

where the given function $f : \Omega \times \mathbb{R}_{>0} \to \mathbb{R}$ models the nonhomogeneity. This can be understood to model the source of material and an example is given by the Fisher-Kolmogoroff equation in section 3.1.1 (c.f Grindrod [18], Murray [42], Okubo [44]).

In a next step, $f : \mathbb{R}^n \to \mathbb{R}$, so $f \in C^\infty(\mathbb{R}^n)$, can be seen as a smooth reaction term, which yields

$$\frac{\partial u}{\partial t} = \Delta u + f(u), \tag{3.3}$$

now with boundary conditions on $\partial\Omega$. Considering $f = f(u, \Delta u, x, t)$, provides us with the semi-linear parabolic *reaction-diffusion equation*

$$\frac{\partial u}{\partial t} = \Delta u + f. \tag{3.4}$$

Following Lam [31], equation (3.4) can be applied to model the evolution of a population.

As outlined in Evans [11, p. 534ff] and Murray [42, p. 400ff], when relaxing the dependence of f such that $f = f(u)$, but defining $f : \mathbb{R}^n \to \mathbb{R}^n$ to be Lipschitz continuous, we can regard a *reaction-diffusion system*

$$\begin{cases} \dfrac{\partial u}{\partial t} - \Delta u = f(u), & \text{in } \Omega \times (0, T] \\ u = 0, & \text{on } \partial\Omega \times [0, T] \\ u = g, & \text{on } \Omega \times \{t = 0\}. \end{cases} \tag{3.5}$$

Now let $\Omega \in \mathbb{R}^n$ be open and bounded, with smooth boundary. And let $u = (u^1, \ldots, u^m)$ and $g \in H_0^1(\Omega, \mathbb{R}^m)$, $g = (g^1, \ldots, g^m)$. Here, we have the Hilbert space $H_0^1(\Omega)$, which is defined via the Sobolev space $W^{1,2}(\Omega)$ such that $H_0^1(\Omega) = W_0^{1,2}(\Omega)$. $W^{1,2}(\Omega)$ denotes the space of functions $u \in W^{1,2}(\Omega) : u = 0$ on $\partial\Omega$, for $W_0^{1,2}(\Omega)$ denoting the closure of $C_c^\infty(\Omega)$ in $W^{1,2}(\Omega)$. $W^{1,2}(\Omega)$ contains all locally summable functions $u : \Omega \to \mathbb{R}$ such that for each multiindex $\alpha : |\alpha| \leq 1$ and $D^\alpha u$ exists in the weak sense and belongs to $L^2(\Omega)$. $C_c^\infty(\Omega)$ describes the space of infinitely differentiable functions $\varphi : \Omega \to \mathbb{R}$ with compact support in Ω (cf. Evans [11, Ch. 5]).

3.1.1 The Fisher-Kolmogoroff equation

An example of the above is given by the *Fisher-Kolmogoroff equation*.We consider the one dimensional case of the *Fisher-Kolmogoroff equation*:

$$\begin{cases} \dfrac{\partial u}{\partial t} - \dfrac{\partial^2 u}{\partial x^2} = u(r(x,t) - u), & \text{for } x \in \mathbb{R}, \text{ and } t > 0, \\ u(x, 0) = u_0(x), & \text{for } x \in \mathbb{R}, \end{cases} \tag{3.6}$$

with $u_0 \in C(\mathbb{R})$ bounded, nonnegative, nontrivial and with compact support. Here, $r : \mathbb{R} \times \mathbb{R} \to \mathbb{R}$ describes the growth rate of the population (cf. Fisher [12], Lam [31] and Murray [42]). The *Fisher-Kolmogoroff equation* provides the basis for the Alfonso et al. [5] model of the migration-proliferation dichotomy in glioma cells, which we study in chapter 4.

Before proceeding to explain how balance laws form the basis for reaction-diffusion systems, we give a short analysis of the Fisher-Kolmogoroff equation and propagating wave solutions in the one-dimensional case. For this purpose, we consider the works of Grindrod [18], Murray [42] and Okubo et al. [44].

Compared to diffusion equations, reaction-diffusion equations allow for travelling wave solutions. Following Murray [42], a travelling wave moves in the domain without change of shape. Consider $u(x,t)$ being a solution of our reaction-diffusion equation, so

$$u(x,t) = u(x-ct) = u(z), \qquad z = x - ct. \tag{3.7}$$

This describes a travelling wave, propagating in positive x-direction with speed $c = \text{const}$. Searching for travelling wave solutions yields ordinary differential equations

$$\frac{\partial u}{\partial t} = -c\frac{du}{dz} \quad \text{and} \quad \frac{\partial u}{\partial x} = \frac{du}{dz}. \tag{3.8}$$

We now describe propagating wave solutions for the Fisher-Kolmogoroff equation. Following Murray [42], we consider an even simpler case, namely

$$\frac{\partial u}{\partial t} = D\frac{\partial^2 u}{\partial x^2} + ku(1-u), \qquad D,k > 0. \tag{3.9}$$

Here, D describes the diffusion parameter and k the parameter for the reaction kinetics. Re-scaling, with $t^* = kt$ and $x^* = x\sqrt{k/D}$ and omitting the asterisk, provides the dimensionless form

$$\frac{\partial u}{\partial t} = \frac{\partial^2 u}{\partial x^2} + u(1-u), \tag{3.10}$$

which has the unstable steady state, $u = 0$, and the stable one, $u = 1$. This can be shown in the following way: Consider a small perturbation, $\varepsilon\eta(x,t)$, around the respective steady state $u_s(x,t)$:

$$u(x,t) = u_s(x,t) + \varepsilon\eta(x,t), \tag{3.11}$$

where $\eta(x,t)$ describes the perturbation term and $\varepsilon > 0$ is a small parameter. This provides us with

$$\begin{aligned} \frac{\partial(u_s+\varepsilon\eta)}{\partial t} &= \frac{\partial^2(u_s+\varepsilon\eta)}{\partial x^2} + (u_s+\varepsilon\eta)(1-(u_s+\varepsilon\eta)), \\ &= \frac{\partial^2 u_s}{\partial x^2} + \varepsilon\frac{\partial^2\eta}{\partial x^2} + u_s + \varepsilon\eta - u_s^2 - 2u_s\varepsilon\eta - \varepsilon^2\eta^2. \end{aligned} \tag{3.12}$$

This term includes the Fisher-Kolmogoroff equation for the steady state

$$\frac{\partial u_s}{\partial t} = \frac{\partial^2 u_s}{\partial x^2} + u_s(1-u_s), \tag{3.13}$$

and provides us with a reaction-diffusion equation for the perturbation term:

$$\varepsilon\frac{\partial\eta}{\partial t} = \varepsilon\frac{\partial^2\eta}{\partial x^2} + \varepsilon\eta - 2u_s\varepsilon\eta - \varepsilon^2\eta^2. \tag{3.14}$$

So we can look at the steady states $u_{s,1} = 0$ and $u_{s,2} = 1$. Inserting $u_{s,1} = 0$ in equation 3.14 yields

$$\begin{aligned} \frac{\partial \eta}{\partial t} &= \frac{\partial^2 \eta}{\partial x^2} + \eta - \varepsilon \eta^2, \\ &\approx \frac{\partial^2 \eta}{\partial x^2} + \eta, \end{aligned} \tag{3.15}$$

since ε is small. The eigenvalues are positive, indicating an unstable steady state.

Now we insert $u_{s,2} = 1$ in equation 3.14. This provides us with

$$\begin{aligned} \frac{\partial \eta}{\partial t} &= \frac{\partial^2 \eta}{\partial x^2} + \eta - 2\eta - \varepsilon \eta^2, \\ &\approx \frac{\partial^2 \eta}{\partial x^2} - \eta, \end{aligned} \tag{3.16}$$

since ε is small. The eigenvalues are negative, indicating a stable steady state (c.f. Murray [42] and Okubo et al. [44]).

Now we turn to travelling wavefront solutions. Travelling wavefront solutions might exist for $0 \leq u \leq 1$, connecting the steady states. If they exist, they show the form

$$u(x,t) = U(z), \qquad z = x - ct, \tag{3.17}$$

and combining the above provides us with

$$-c\frac{\partial U}{\partial z} = \frac{\partial^2 U}{\partial z^2} + U(1-U). \tag{3.18}$$

Typically, a solutions reaches the respective steady states at $z \to \pm\infty$, providing us with an eigenvalue problem for a non-negative U, such that we have

$$\lim_{z\to\infty} U(z) = 0, \quad \text{and} \quad \lim_{z\to-\infty} U(z) = 1. \tag{3.19}$$

For example, this resembles a tumour starting to spread from the origin at one end of the domain and propagating over the domain.

Now let

$$\frac{\partial U}{\partial z} = V, \quad \text{and} \quad \frac{\partial V}{\partial z} = -cV - U(1-U), \tag{3.20}$$

and we describe equation (3.18) in the phase plane (U, V). We obtain the trajectories:

$$\frac{dV}{dU} = \frac{-cV - U(1-U)}{V}. \tag{3.21}$$

Equation (3.21) has singular points (U_s, V_s), if

$$-cV_s - U_s(1-U_s) = V_s = 0 \tag{3.22}$$

holds. So $V_s = 0$ and we obtain the singular points at $(U, V) = (0, 0)$ and at $(U, V) = (1, 0)$.

We now want to analyse the stability of the singular points. Therefore, we build the Jacobian matrix:

$$J(U,V) = \begin{pmatrix} \frac{\partial V}{\partial U} & \frac{\partial V}{\partial V} \\ \frac{\partial V'}{\partial U} & \frac{\partial V'}{\partial V} \end{pmatrix} = \begin{pmatrix} 0 & 1 \\ -1 + 2U & -c \end{pmatrix}, \tag{3.23}$$

where we use $V' = \frac{\partial V}{\partial z}$.

For the singular point $(U, V) = (0, 0)$ we obtain

$$J(0,0) = \begin{pmatrix} 0 & 1 \\ -1 & -c \end{pmatrix}, \tag{3.24}$$

which has the eigenvalues

$$\begin{vmatrix} -\lambda & 1 \\ -1 & -c - \lambda \end{vmatrix} = 0 \quad \Rightarrow \quad \lambda_{1,2} = \frac{-c \pm \sqrt{c^2 - 4}}{2}, \tag{3.25}$$

providing a stable node for $c^2 > 4$, a degenerate node for $c = c_{min} = 2$, and a stable spiral for $c^2 < 4$.

For the singular point $(U, V) = (1, 0)$ we obtain

$$J(0,0) = \begin{pmatrix} 0 & 1 \\ 1 & -c \end{pmatrix}, \tag{3.26}$$

which has the eigenvalues

$$\begin{vmatrix} -\lambda & 1 \\ 1 & -c - \lambda \end{vmatrix} = 0 \quad \Rightarrow \quad \lambda_{1,2} = \frac{-c \pm \sqrt{c^2 + 4}}{2}, \tag{3.27}$$

providing a saddle point.

Turning back to the original Fisher-Kolmogoroff equation (3.6), before re-scaling, we obtain wavespeeds of

$$c \geq c_{min} = 2\sqrt{kD}, \tag{3.28}$$

which depends on the diffusion parameter, D, and the parameter for the reaction kinetics, k (c.f. Kuznetsov et al. [30], or Murray [42]).

Turning now to initial conditions $u(x, 0)$, the question arises which conditions allow for travelling wave solutions. Kolmogoroff et al. [29] and Murray [42] describe that for $u(x, 0)$ with compact support,

$$u(x,0) = u_0(x) \geq 0, u_0(x) = \begin{cases} 1, & \text{if } x \leq x_1 \\ 0, & \text{if } x \geq x_2 \end{cases}, \tag{3.29}$$

with $x_1 < x_2$, and $u_0(x)$ continuous in $x \in [x_1, x_2]$, we obtain a travelling wavefront solution $U(z) = U(x - 2t)$. So we have a travelling wavefront solution propagating with minimum speed $c_{min} = 2$. For different initial data, the behaviour of $u(x, 0)$, $x \to \pm\infty$, is the deciding factor.

This can be seen in the example described by Mollison [40]. We linearise the Fisher-Kolmogoroff equation (3.10), assuming u small, hence $u^2 \ll u$. This provides us with

$$\frac{\partial u}{\partial t} = u + \frac{\partial^2 u}{\partial x^2}. \tag{3.30}$$

We are interested in travelling wave solutions of the form

$$u(x, t) = A \exp(-a(x - ct)), \tag{3.31}$$

considering $u(x, 0) \sim A \exp(-ax)$ for $x \to \infty$, $a > 0$ and $A > 0$ arbitrary. Using equation (3.31) to solve equation (3.30) provides us with

$$acu(x, t) = u + (-a)^2 u(x, t). \tag{3.32}$$

which yields the dispersion relation

$$ac = 1 + a^2 \quad \Rightarrow \quad c = a + \frac{1}{a}. \tag{3.33}$$

So $c_{min} = 2$ is achieved for $a = 1$. We obtain the solution

$$u(x, t) = A \exp(-x + 2t). \tag{3.34}$$

For $a > 0$, $a \neq 1$. The waves propagate with $c > 2$.

Still assuming $x > 0$, such that $u^2 \ll u$, we describe the leading edge of our travelling wavefront solution. For $\min[\exp(-ax), \exp(-x)]$, we consider two cases:

$$a < 1 \quad \Rightarrow \quad \exp(-ax) > \exp(-x), \tag{3.35}$$

and according to equation (3.33), we have $c > 2$ and the leading edge of the wave controls the velocity. For

$$a > 1 \quad \Rightarrow \quad \exp(-ax) < \exp(-x), \tag{3.36}$$

we see that $\exp(-ax)$ is strictly smaller than $\exp(ax)$ and follows the wavefront with $c = 2$. Overall, we get

$$c = a + \frac{1}{a}, \quad \text{for} \quad 0 < a \leq 1, \quad \text{and} \quad c = 2, \quad \text{for } a \geq 1. \tag{3.37}$$

3.1.2 Balance laws form the basis for reaction-diffusion systems

Following Grindrod [18, p. 6ff], we explain the connection between balance laws and reaction-diffusion systems. Here, we consider the density of a given entity, so for example of a population or a concentration, to describe the distribution of elements of said entity. Let $c : \Omega \times \mathbb{R}_{\geq 0} \to \mathbb{R}$, for $\Omega \subset \mathbb{R}^n$ open, be the particle density function. Consider further $Q(x,t)$, the net creation rate of particles at each point $x \in \Omega$, and the flux density $J(x,t)$ and regard a subset $B \subseteq \Omega$. We obtain the mass of our population in the volume B via

$$\int_B c dx, \tag{3.38}$$

for $x = (x_1, \ldots, x_n)^T$ relying on Cartesian coordinates. The balance law then states that over time, the change of mass in the volume B equals the rate of flow across the boundary in addition to any matter created inside B. So

$$\frac{\partial}{\partial t} \int_B c dx = - \int_{\partial B} J \cdot n dA + \int_B Q dx, \tag{3.39}$$

for n being the unit outer normal vector in $\mathbb{R}^n$. If $J \in C^1$, the divergence theorem can be applied and we obtain

$$\int_B \frac{\partial c}{\partial t} dx = \int_B -\nabla J + Q dx. \tag{3.40}$$

Since B is chosen arbitrarily, we obtain the balance law

$$\frac{\partial c}{\partial t} = -\nabla J + Q. \tag{3.41}$$

Referencing Grindrod [18] and Okubo [44], an example is given by following Fick's law with

$$J = -D \nabla c, \tag{3.42}$$

where D denotes the diffusion coefficient. So we arrive at

$$\frac{\partial c}{\partial t} = D \Delta c + Q(x,t,c), \tag{3.43}$$

assuming D constant. The one-dimensional case has the solution

$$c(x,t) = \frac{M}{2(\pi D t)^{1/2}} \exp\left(\frac{-x^2}{4Dt}\right), \tag{3.44}$$

assuming that no matter is created inside the volume B. So $Q(x,t,c) = 0$, with initially $c(x,0) = M$ and working on the whole real line, for $M \in \mathbb{R}_{\geq 0}$.

3.1.3 Deriving the diffusion equation from a simple random walk approach

We follow the explanations in Murray [42], Okubo [44] and Cantrell [9] to provide a simplified derivation of the diffusion equation from a simple random walk approach.

Starting with a discrete setup, we consider the one dimensional, horizontal, motion of a particle. At each time step Δt, the particle goes one step Δx either to the left or to the right. So after time $N\Delta t$, $N \in \mathbb{N}$, a particle can be found in the interval $[-N\Delta x, N\Delta x]$. We obtain the probability $p(m,n)$ that a particle is at a point m steps to the right after n time-steps:

$$p(m,n) = \left(\frac{1}{2}\right)^n \frac{n!}{[(n+m)/2]![(n-m)/2]!} = \left(\frac{1}{2}\right)^2 \frac{n!}{a!b!}, \tag{3.45}$$

for $m = a - b, n = a + b$, where a, b denote the number of steps to the right, or to the left respectively. The probability $p(m,n)$ is obtained since we have a total of $\frac{n!}{a!b!}$ possibilities to arrive at a point $x = m\Delta x$, for a total of 2^n paths in n time-steps.

Equation (3.45) follows a Bernoulli distribution. For the case of the number of time steps n becoming large, so $n + m$ becomes large as well, we arrive at a Gaussian probability distribution:

$$\lim_{n\to\infty} p(m,n) \sim \left(\frac{2}{\pi n}\right)^{1/2} \exp\left(\frac{-m^2}{2n}\right), \tag{3.46}$$

since in the asymptotic case, we have

$$n! = \Gamma(n+1) = \int_0^\infty \exp(-t)t^n dt, \tag{3.47}$$

where $\Gamma(\cdot)$ denotes the gamma function. This gives us Stirling's formula

$$n! \sim (2\pi n)^{1/2} n^n \exp(-n), \tag{3.48}$$

for $n \gg 1$.

We now pass to the continuous case starting from equation (3.46):

$$\frac{p(\frac{x}{\Delta x}, \frac{t}{\Delta t})}{2\Delta x} \sim \left(\frac{\Delta t}{2\pi t(\Delta x)^2}\right)^{1/2} \exp\left(-\frac{x^2}{2t}\frac{\Delta t}{(\Delta x)^2}\right). \tag{3.49}$$

The probability to find a given particle in the interval $(x, x + \Delta x)$, at time t, is given by:

$$u(x,t) = \lim_{\substack{\Delta x\to 0\\ \Delta t\to 0}} \frac{p(\frac{x}{\Delta x}, \frac{t}{\Delta t})}{2\Delta x} = \left(\frac{1}{4\pi Dt}\right)^{1/2} \exp\left(\frac{-x^2}{4Dt}\right), \tag{3.50}$$

where

$$D := \lim_{\substack{\Delta x \to 0 \\ \Delta t \to 0}} \frac{(\Delta x)^2}{2\Delta t} \neq 0, \tag{3.51}$$

is known as the diffusion coefficient , respectively the diffusivity. As explained in Murray [42], the diffusion coefficient describes an 'efficiency' measure regarding the dispersion of particles from high to low density.

A slight variant of this idea is obtained from Murray [42] and Okubo [44]. We derive the diffusion equation as an extension of the random walk approach outlined above. We rewrite the probability to find a particle at a point in space and time (x, t) as

$$p(x,t) = \alpha p(x - \Delta x, t - \Delta t) + \beta p(x + \Delta x, t - \Delta t), \tag{3.52}$$

for the probabilities α, β, that a particle moves to the right, respectively to the left, at time-step Δt. It holds that $\alpha + \beta = 1$. Taylor-expanding equation (3.52), assuming $x \gg \Delta x, t \gg \Delta t$, and evaluating at (x, t) provides us with

$$\begin{aligned} p(x - \Delta x, t - \Delta t) = p(x,t) &- \Delta x \frac{\partial p}{\partial x} - \Delta t \frac{\partial p}{\partial t} \\ &+ \frac{(\Delta x)^2}{2} \frac{\partial^2 p}{\partial x^2} \\ &+ (\Delta x \Delta t) \frac{\partial^2 p}{\partial x \partial t} + \frac{(\Delta t)^2}{2} \frac{\partial^2 p}{\partial t^2} \\ &- \frac{(\Delta x)^3}{6} \frac{\partial^3 p}{\partial x^3} - \frac{(\Delta x)^2 \Delta t}{2} \frac{\partial^3 p}{\partial x^2 \partial t} \\ &- \frac{(\Delta x)(\Delta t)^2}{2} \frac{\partial^3 p}{\partial x \partial t^2} - \frac{(\Delta t)^3}{6} \frac{\partial^3 p}{\partial t^3} \\ &+ O(4), \end{aligned} \tag{3.53}$$

and

$$\begin{aligned} p(x + \Delta x, t - \Delta t) = p(x,t) &+ \Delta x \frac{\partial p}{\partial x} - \Delta t \frac{\partial p}{\partial t} \\ &+ \frac{(\Delta x)^2}{2} \frac{\partial^2 p}{\partial x^2} - (\Delta x \Delta t) \frac{\partial^2 p}{\partial x \partial t} + \frac{(\Delta t)^2}{2} \frac{\partial^2 p}{\partial t^2} \\ &+ \frac{(\Delta x)^3}{6} \frac{\partial^3 p}{\partial x^3} - \frac{(\Delta x)^2 \Delta t}{2} \frac{\partial^3 p}{\partial x^2 \partial t} \\ &+ \frac{(\Delta x)(\Delta t)^2}{2} \frac{\partial^3 p}{\partial x \partial t^2} - \frac{(\Delta t)^3}{6} \frac{\partial^3 p}{\partial t^3} \\ &+ O(4), \end{aligned} \tag{3.54}$$

where $O(4)$ describes terms of order 4 and higher.

Defining $\varepsilon := \alpha - \beta$ and using $\alpha + \beta = 1$, we obtain

$$\begin{aligned}\frac{\partial p}{\partial t} = &-\frac{\varepsilon \Delta x}{\Delta t}\frac{\partial p}{\partial x} + \frac{(\Delta x)^2}{2\Delta t}\frac{\partial^2 p}{\partial x^2} + \varepsilon \Delta x \frac{\partial^2 p}{\partial x \partial t} + \frac{\Delta t}{2}\frac{\partial^2 p}{\partial t^2} \\ &- \frac{\varepsilon}{\Delta t}\frac{(\Delta x)^3}{6}\frac{\partial^3 p}{\partial x^3} - \frac{(\Delta x)^2}{2}\frac{\partial^3 p}{\partial x^2 \partial t} \\ &- \varepsilon \frac{\Delta x \Delta t}{2}\frac{\partial^3 p}{\partial x \partial t^2} - \frac{(\Delta t)^2}{6}\frac{\partial^3 p}{\partial t^3} + O(4).\end{aligned} \tag{3.55}$$

So further defining $u := \lim_{\Delta x, \Delta t, \varepsilon \to 0} \frac{\varepsilon \Delta x}{\Delta t}$ and regarding equation (3.55) for the limit cases $\Delta x, \Delta t \to 0$, we arrive at the diffusion equation

$$\frac{\partial p}{\partial t} = -u\frac{\partial p}{\partial x} + D\frac{\partial^2 p}{\partial x^2}. \tag{3.56}$$

For the isotropic case $\alpha = \beta = 1/2$, which represents the case of an unbiased random walk, we obtain the diffusion equation

$$\frac{\partial p}{\partial t} = D\frac{\partial^2 p}{\partial x^2}, \tag{3.57}$$

where D is defined as in equation (3.51).

Chapter 4

Modelling the Migration-Proliferation Dichotomy - The Alfonso et al. Model

In this chapter, we explain the Alfonso et al. [5] model for the migration-proliferation dichotomy. The underlying assumptions are described in chapter 2. At first, we describe the general idea and rebuild the system of equations that is used to express the characteristics of the migration-proliferation dichotomy. We provide a numerical analysis of the model and describe the results. A discussion and an outlook for subsequent works is provided in chapter 5.

4.1 Description

The model in Alfonso et al. [5] describes the feedback mechanisms between glioma cells and the brain vasculature. Of particular interest are the proliferation-migration dichotomy, the vaso-occlusion at the tissue borders and the interaction of these factors. The underlying assumptions are listed in section 2.3.

Following Alfonso et al. [5], we describe the model using the density of glioma cells, the pro-angiogenic factor concentration, the density of functional tumour vasculature and the oxygen concentration:

$$\rho, a, \nu, \sigma : \mathbb{R}^d \times \mathbb{R} \to \mathbb{R}, \tag{4.1}$$

for dimension $d \in \{1, 2, 3\}$.

4.1.1 Density of glioma cells

The density $\rho(x, t)$ of glioma cells is modelled to account for the phenotype duality of a migratory type, $\rho_1(x, t)$, respectively for a proliferative type, $\rho_2(x, t)$, given the oxygen concentration $\sigma(x, t)$ in the hypoxic, respectively

normoxic environment. As outlined, glioma cells switch phenotypes to adapt to their surroundings. This process is assumed to be linear and follows

$$f_{21}(\sigma) = \lambda_1 - \sigma, \quad f_{12}(\sigma) = \lambda_2 \sigma, \quad \text{with } \lambda_{1,2} > 0, \tag{4.2}$$

from a migratory to a proliferative type, respectively the other way around. The parameters $\lambda_{1,2}$ describe the proliferative to migratory, respective migratory to proliferative, phenotypic switching parameters. Furthermore, we model the cell motility as a diffusive process, whereas the cell proliferation is assumed to follow a logistic growth term. This will lead us to a generalised Fisher-Kolmogorov equation (4.8) in the description of growth and invasive behaviour of the population of glioma cells.

In the following, and in the following subsections, the space and time variables (x, t) are omitted for ease of readability. We have

$$\frac{\partial \rho_1}{\partial t} = D_\rho \nabla^2 \rho_1 - f_{12}(\sigma)\rho_1 + f_{21}(\sigma)\rho_2, \tag{4.3}$$

and

$$\frac{\partial \rho_2}{\partial t} = b_\rho \rho_2 \left(1 - \frac{\rho_1 + \rho_2}{N}\right) + f_{12}(\sigma)\rho_1 - f_{21}(\sigma)\rho_2, \tag{4.4}$$

where we describe the diffusion and proliferation coefficients via D_ρ and b_ρ. The carrying capacity of the brain tissue is given by N. It holds that $D_\rho, b_\rho, N > 0$.

Under the assumption that the switching of the phenotypes occurs at a faster rate than cell division and cell motility, we have $f_{12}(\sigma)\rho_1 = f_{21}(\sigma)\rho_2$. We consider the total density of glioma cells:

$$\rho = \rho_1 + \rho_2 = \left(1 + \frac{f_{12}(\sigma)}{f_{21}(\sigma)}\right)\rho_1 = \left(1 + \frac{f_{21}(\sigma)}{f_{12}(\sigma)}\right)\rho_2, \tag{4.5}$$

Given

$$\rho_1 = \frac{f_{21}(\sigma)}{f_{12}(\sigma) + f_{21}(\sigma)}\rho \tag{4.6}$$

and

$$\rho_2 = \frac{f_{12}(\sigma)}{f_{12}(\sigma) + f_{21}(\sigma)}\rho, \tag{4.7}$$

we obtain

$$\frac{\partial \rho}{\partial t} = \frac{\partial(\rho_1 + \rho_2)}{\partial t} = D_\rho \nabla^2(\alpha(\sigma)\rho) + b_\rho(\beta(\sigma)\rho)(1 - \frac{\rho}{N}). \tag{4.8}$$

Here we use

$$\alpha(\sigma) = \frac{f_{21}(\sigma)}{f_{12}(\sigma) + f_{21}(\sigma)} = \frac{\lambda_1 - \sigma}{(\lambda_2 - 1)\sigma + \lambda_1}, \tag{4.9}$$

and

$$\beta(\sigma) = \frac{f_{12}(\sigma)}{f_{12}(\sigma) + f_{21}(\sigma)} = \frac{\lambda_2 \sigma}{(\lambda_2 - 1)\sigma + \lambda_1} \tag{4.10}$$

with

$$1 = \alpha(\sigma) + \beta(\sigma). \tag{4.11}$$

With the physiological oxygen concentration σ_0 in the normal brain tissue, we can provide normalised coefficients for diffusion, $D_\rho = \frac{D}{\alpha(\sigma_0)}$, and proliferation, $b_\rho = \frac{b}{\beta(\sigma_0)}$. For a constant oxygen concentration, $\sigma(x,t) = \sigma_0$, we obtain

$$\frac{\partial \rho}{\partial t} = D\nabla^2 \rho + b\rho(1 - \frac{\rho}{N}), \tag{4.12}$$

which is the classical Fisher-Kolmogorov equation as provided in equation (3.6). The boundary conditions will be discussed in subsection 4.1.5.

4.1.2 Pro-angiogenic factor concentration

The pro-angiogenic factor concentration $a(x,t)$ is responsible for stimulating neovascularisation, which describes the process of forming new blood vessels, via a plethora of mechanisms. These mechanisms are still to be understood and Alfonso et al. [5] simplify the model to only account for a generic concentration of pro-angiogenic factors.

The formation of tumour vasculature then takes place if the concentration of pro-angiogenic factors exceeds the concentration of anti-angiogenic factors in a given environment. Pro-angiogenic factors are assumed to form only in a hypoxic environment. As outlined above, endothelial cells, the cells forming the vascular network, absorb pro-angiogenic factors. This leads us to

$$\frac{\partial a}{\partial t} = D_a \nabla^2 a + k_1 \rho \tilde{H}_\theta(\sigma - \sigma_a^*) - k_2 a v - k_3 a. \tag{4.13}$$

Analogously, D_a describes the diffusion coefficient of the pro-angiogenic factor concentration and $k_{1,2,3}$ capture the rates of production, consumption and the natural decay of pro-angiogenic factors. Furthermore, $\sigma_a^* \in (0, \sigma_0)$ describes the threshold for the hypoxic oxygen concentration.

With $\tilde{H}_\theta(\sigma - \sigma_a^*)$ we have a continuous approximation of the Heaviside decreasing step function $H(\xi) : H(\xi \leq 0) = 1$ and $H(\xi > 0) = 0$. In particular,

$$\tilde{H}_\theta(\sigma - \sigma_a^*) = 1 - \frac{1}{1 + e^{-2\theta(\sigma - \sigma_a^*)}}, \tag{4.14}$$

with θ the factor that controls the steepness of the Heaviside function.

Glioma cells produce pro-angiogenic factors in a hypoxic environment, so $\sigma \leq \sigma_a^*$, which is described by the Heaviside step function. We assume a

quasi-steady state approximation for the pro- angiogenic factor concentration in equation (4.13), so:

$$a = \frac{k_1 \rho \tilde{H}_\theta(\sigma - \sigma^*)}{k_2 \nu + k_3}. \tag{4.15}$$

4.1.3 Density of functional tumour vasculature

The model at hand follows a simplified approach, accounting only for functional vasculature and describing the density of functional tumour vasculature $\nu(x,t)$ as a normalised and dimensionless quantity. So the case of $\nu = 0$ describes avascular tissue, $\nu = 1$ excessive vascularisation in a hypothetical case, and we consider normal brain tissue for $\nu = 1/2$.

The formation of new blood vessels occurs when the concentration of pro-angiogenic factors exceeds the concentration of anti-angiogenic factors. This is the case if $a(x,t) > 0$.

This formation process is assumed to follow a logistic growth term. Furthermore, the generation of functional tumour blood vessels follows the Michael-Menten kinetics, assuming that endothelial cells are dispersed at a constant rate. The occlusion or collapse of blood vessels is promoted by mechanical or chemical signals in an environment with a high density of glioma cells. Taking into account a power law dependency of the vaso-occlusion with respect to the glioma cell density, we arrive at

$$\frac{\partial \nu}{\partial t} = D_\nu \nabla^2 \nu + g_1 \frac{a}{\mu + a} \nu(1 - \nu) - g_2 \nu \rho^n. \tag{4.16}$$

Analogously, D_ν describes the diffusion coefficient of the net dispersal of tumour vasculature, g_1 captures the formation rate of functional blood vessels and g_2 the vaso-occlusion rate. μ describes the pro-angiogenic factor concentration at which g_1, the vasculature formation, rate is half-maximal. This will be captured in $K = \mu \frac{k_2}{k_1}$, which represents the concentration of pro-angiogenic factors at half-maximal formation rate of functional tumour vasculature. The parameter n is introduced to regulate the degree of blood vessel occlusion, depending on the density of glioma cells. The vaso-occlusion term $g_2 \nu \rho^n$ captures the mechanical pressure that is exerted on blood vessels in regions of high glioma cell density. For surpassing a certain threshold of intratumoural cellular pressure, tumour blood vessels collapse in a substantial fashion. We assume vasoocclusion only for $\rho > N/2$, when half of the brain tissue carrying capacity is surpassed. We have $D_\nu, g_1, \mu, g_2, n > 0$. With equation (4.15) and $k_3 \ll k_2$, so the concentration of pro-angiogenic factors decaying at a

smaller rate compared to the uptake rate by endothelial cells, we obtain

$$\begin{aligned}\frac{\partial \nu}{\partial t} &= D_\nu \nabla^2 \nu + g_1 \frac{k_1 \rho \tilde{H}_\theta(\sigma - \sigma_a^*)}{\mu(k_2\nu + k_3) + g_1 k_1 \tilde{H}_\theta(\sigma - \sigma_a^*)} \nu(1-\nu) - g_2 \nu \rho^n \\ &= D_\nu \nabla^2 \nu + g_1 \frac{\frac{\rho}{\nu}\tilde{H}_\theta(\sigma - \sigma_a^*)}{K + \frac{\rho}{\nu}\tilde{H}_\theta(\sigma - \sigma_a^*)} \nu(1-\nu) - g_2 \nu \rho^n.\end{aligned} \tag{4.17}$$

4.1.4 Oxygen concentration

Functional blood vessels are required for the delivery of oxygen into the brain. Within tissues, transport occurs by diffusion and convection. Following the Alfonso et al. [5] model, we focus only on diffusion processes. So we describe the oxygen concentration via

$$\frac{\partial \sigma}{\partial t} = D_\sigma \nabla^2 \sigma + h_1 \nu(\sigma_0 - \sigma) - h_2 \rho \sigma. \tag{4.18}$$

Analogously, D_σ describes the oxygen diffusion coefficient, h_1 the permeability coefficient of functional vasculature, and h_2 the oxygen consumption rate of glioma cells. The supply rate is related to the functional vasculature and the difference between physiological oxygen concentration in normal brain tissue σ_0 and in tumour interstitium.

4.1.5 Model formulation, boundary and initial conditions

Given the above, we arrive at the system of coupled PDEs:

$$\begin{aligned}\frac{\partial \rho}{\partial t} &= D_\rho \nabla^2(\alpha(\sigma)\rho) + b_\rho \beta(\sigma)\rho(1 - \rho/N) \\ \frac{\partial \nu}{\partial t} &= D_\nu \nabla^2 \nu + g_1 \frac{\frac{\rho}{\nu}\tilde{H}_\theta(\sigma - \sigma_a^*)}{K + \frac{\rho}{\nu}\tilde{H}_\theta(\sigma - \sigma_a^*)} \nu(1-\nu) - g_2 \nu \rho^n \\ \frac{\partial \sigma}{\partial t} &= D_\sigma \nabla^2 \sigma + h_1 \nu(\sigma_0 - \sigma) - h_2 \rho \sigma.\end{aligned} \tag{4.19}$$

This provides us with a closed system, assuming the initial conditions

$$\begin{aligned}\rho(x,0) &= \rho_0 \tilde{H}_\gamma(x - \varepsilon) = \rho_0 \left(1 - \frac{1}{1 + e^{-2\gamma(x-\varepsilon)}}\right), && x \in [0, L], \\ \nu(x,0) &= \nu_0, && x \in [0, L], \\ \sigma(x,0) &= \sigma_0, && x \in [0, L],\end{aligned} \tag{4.20}$$

where γ controls the steepness of $\tilde{H}_\gamma$ at position $(x - \varepsilon)$. The initial densities are provided by ρ_0, σ_0 and ν_0. We have $\varepsilon > 0$, and $L > 0$ the length of the one dimensional computational domain. As well, the model only accounts

for an isolated host tissue, so the system behaviour is only due to the above dynamics. So we have the no-flux boundary conditions:

$$\begin{aligned} \rho_x(0,t) = \nu_x(0,t) &= \sigma_x(0,t) = 0, \qquad 0 \leq t \leq T_f \\ \rho_x(L,t) = \nu_x(L,t) &= \sigma_x(L,t) = 0, \qquad 0 \leq t \leq T_f, \end{aligned} \tag{4.21}$$

for an arbitrary simulation time $T_f > 0$.

In the following, we analyse two versions of this system of coupled PDEs. These are referred to as "Model I" and "Model III" in the work of Alfonso et al. [5]. The first model, from now on referred to as the "Baseline Cell Density Model", assumes the vascular density, $\nu(x,t) = \nu_0$, and the oxygen concentration, $\sigma(x,t) = \sigma_0$, to be constant and reduces to a single PDE. The "Interplay model", or "Model III", considers the full system of equations (4.19).

4.2 Numerical Analysis

For the numerical analysis, we follow the work of Alfonso et al. [5] using the same parameters. These are summarized in table 4.1.

The initial value problem is implemented in python (Version 3.9.7). The system of partial differential equations is solved, relying on python's scipy package [51]. In particular, we employ the solve_ivp function, using an explicit Runge-Kutta method of order five. We solve the initial value problem on a one dimensional domain of length $L = 200$mm and over a time-span of $T = 1000$ days.

We compute the "Baseline Cell Density Model" (see subsection 4.2.1) and the "Interplay Model" (see subsection 4.2.2). The code is attached in the appendix C[1]. So we show numerical solutions for the baseline Fisher-Kolmogoroff model for glioma cell density and solutions for the complete model for glioma cell density, oxygen concentration and density of functional vasculature.

4.2.1 Fisher-Kolmogoroff Cell Density Model

We start with a simplified version of system (4.19), assuming both the vascular density, $\nu(x,t) = \nu_0$, and the oxygen concentration, $\sigma(x,t) = \sigma_0$, to be constant. This provides us with the classical Fisher-Kolmogoroff equation for the glioma cell density:

$$\frac{\partial \rho}{\partial t} = D\nabla^2\rho + b\rho(1 - \frac{\rho}{N}), \tag{4.22}$$

where we use

$$D = D_\rho \alpha(\sigma_0) = D_\rho \frac{\lambda_1 - \sigma_0}{(\lambda_2 - 1)\sigma_0 + \lambda_1} \tag{4.23}$$

[1]The code can also be found in the GitHub Repository:
https://github.com/SiebenJ7/Migration-Proliferation-Dichotomy.git.

Table 4.1: Parameters for the model simulation as obtained from the work of Alfonso et al. [5].

Parameter	Description	Value
Glioma cell density $\rho(x,t)$		
D_ρ	Intrinsic diffusion rate of glioma cells	$2.73 \times 10^{-2}\text{mm}^2\ \text{day}^{-1}$
b_ρ	Intrinsic proliferation rate of glioma cells	$2.73 \times 10^{-3}\text{mm}^2\ \text{day}^{-1}$
N	Brain tissue carrying capacity	100 cells mm^{-1}
ρ_0	Initial cell density	40 cells mm^{-1}
λ_1	Proliferative to migratory phenotypic switching parameter	2.0 nmol mm^{-1}
λ_2	Migratory to proliferative phenotypic switching parameter (dimensionless)	1.0
Oxygen concentration $\sigma(x,t)$		
D_σ	Oxygen diffusion rate	$1.51 \times 10^{2}\text{mm}^2\ \text{day}^{-1}$
h_1	Oxygen supply rate	$3.37 \times 10^{-1}\ \text{day}^{-1}$
h_2	Oxygen consumption rate of glioma cells	5.73×10^{-3} mm $\text{cell}^{-1}\ \text{day}^{-1}$
σ_0	Physiological oxygen concentration	1.0 nmol mm^{-1}
Vasculature density $\nu(x,t)$		
D_ν	Vasculature dispersal rate	$5.0 \times 10^{-4}\text{mm}^2\ \text{day}^{-1}$
g_1	Vasculature formation rate	$0.1\ \text{day}^{-1}$
σ_a^*	Oxygen concentration threshold for hypoxia	2.5×10^{-1} nmol mm^{-1}
K	Half-maximal pro-angiogenic factor concentration	1.0 nmol mm^{-1}
g_2	Vaso-occlusion rate	$5.0 \times 10^{-13}\text{cell}^{-n}\text{mm}^{n}\ \text{day}^{-1}$
n	Vaso-occlusion degree (dimensionless)	6
ν_0	Initial density of tumour vasculature (dimensionless)	0.5

and

$$b = b_\rho \beta(\sigma_0) = b_\rho \frac{\lambda_2 \sigma_0}{(\lambda_2 - 1)\sigma_0 + \lambda_1}. \tag{4.24}$$

Basic numerical solutions are provided using finite difference methods. So

we approximate the time and space derivatives using the following:

$$\begin{aligned}\frac{\partial \rho}{\partial t}(t_k, x_j) &\approx \frac{\rho(t_{k+1}, x_j) - \rho(t_k, x_j)}{\Delta t} + O(\Delta t) \\ &\approx \frac{\rho_j^{k+1} - \rho_j^k}{\Delta t} + O(\Delta t),\end{aligned} \tag{4.25}$$

and

$$\begin{aligned}\frac{\partial^2 \rho}{\partial x^2}(t_k, x_j) &\approx \frac{\rho(t_k, x_{j-1}) - 2\rho(t_k, x_j) + \rho(t_k, x_{j+1})}{(\Delta x)^2} + O((\Delta x)^2) \\ &\approx \frac{\rho_{j-1}^k - 2\rho_j^k + \rho_{j+1}^k}{(\Delta x)^2} + O((\Delta x)^2),\end{aligned} \tag{4.26}$$

where ρ_j^k denotes the cell density at time step k and position j.

Combining the above with equation (4.22) gives us the explicit scheme:

$$\frac{\rho_j^{k+1} - \rho_j^k}{\Delta t} = D\frac{\rho_{j-1}^k - 2\rho_j^k + \rho_{j+1}^k}{(\Delta x)^2} + b\rho_j^k\left(1 - \frac{\rho_j^k}{N}\right), \tag{4.27}$$

which we rewrite to obtain:

$$\rho_j^{k+1} = \rho_j^k + \frac{D\Delta t}{(\Delta x)^2}\left(\rho_{j-1}^k - 2\rho_j^k + \rho_{j+1}^k\right) + \Delta t b\rho_j^k\left(1 - \frac{\rho_j^k}{N}\right). \tag{4.28}$$

4.2.2 Interplay Model

Now, neither the vascular density, $\nu(x,t)$, nor the oxygen concentration $\sigma(x,t)$ are assumed to be constant. We analyse the interplay of glioma cell density, oxygen concentration and density of functional tumour vasculature. This provides us with:

$$\begin{aligned}\frac{\partial \rho}{\partial t} &= D_\rho \nabla^2(\alpha(\sigma)\rho) + b_\rho \beta(\sigma)\rho(1 - \rho/N) \\ \frac{\partial \nu}{\partial t} &= D_\nu \nabla^2 \nu + g_1 \frac{\frac{\rho}{\nu}\tilde{H}_\theta(\sigma - \sigma_a^*)}{K + \frac{\rho}{\nu}\tilde{H}_\theta(\sigma - \sigma_a^*)}\nu(1-\nu) - g_2\nu\rho^n \\ \frac{\partial \sigma}{\partial t} &= D_\sigma \nabla^2 \sigma + h_1\nu(\sigma_0 - \sigma) - h_2\rho\sigma.\end{aligned} \tag{4.29}$$

Following Alfonso et al. [5] and taking $\lambda_2 = 1$, we have

$$\begin{aligned}\nabla^2(\alpha(\sigma)\rho) &= \nabla^2\left(\frac{\lambda_1 - \sigma}{\lambda_1}\rho\right) \\ &= \frac{1}{\lambda_1}\nabla\left(\lambda_1\frac{\partial \rho}{\partial x} - \frac{\partial \rho}{\partial x}\sigma - \frac{\partial \sigma}{\partial x}\rho\right) \\ &= \frac{1}{\lambda_1}\left(\lambda_1\frac{\partial^2 \rho}{\partial x^2} - 2\frac{\partial \sigma}{\partial x}\frac{\partial \rho}{\partial x} - \sigma\frac{\partial^2 \rho}{\partial x^2} - \frac{\partial^2 \sigma}{\partial x^2}\rho\right).\end{aligned} \tag{4.30}$$

Again, we start with a finite difference method, approximating the time and space derivatives as follows:

$$\begin{aligned}\frac{\partial \sigma}{\partial t}(t_k, x_j) &\approx \frac{\sigma(t_{k+1}, x_j) - \sigma(t_k, x_j)}{\Delta t} + O(\Delta t) \\ &\approx \frac{\sigma_j^{k+1} - \sigma_j^k}{\Delta t} + O(\Delta t),\end{aligned} \tag{4.31}$$

and

$$\begin{aligned}\frac{\partial^2 \sigma}{\partial x^2}(t_k, x_j) &\approx \frac{\sigma(t_k, x_{j-1}) - 2\sigma(t_k, x_j) + \sigma(t_k, x_{j+1})}{(\Delta x)^2} + O((\Delta x)^2) \\ &\approx \frac{\sigma_{j-1}^k - 2\sigma_j^k + \sigma_{j+1}^k}{(\Delta x)^2} + O((\Delta x)^2).\end{aligned} \tag{4.32}$$

Respectively for the density of functional tumour vasculature:

$$\begin{aligned}\frac{\partial \nu}{\partial t}(t_k, x_j) &\approx \frac{\nu(t_{k+1}, x_j) - \nu(t_k, x_j)}{\Delta t} + O(\Delta t) \\ &\approx \frac{\nu^{k+1} - \nu^k}{\Delta t} + O(\Delta t),\end{aligned} \tag{4.33}$$

and

$$\begin{aligned}\frac{\partial^2 \nu}{\partial x^2}(t_k, x_j) &\approx \frac{\nu(t_k, x_{j-1}) - 2\nu(t_k, x_j) + \nu(t_k, x_{j+1})}{(\Delta x)^2} + O((\Delta x)^2) \\ &\approx \frac{\nu_{j-1}^k - 2\nu_j^k + \nu_{j+1}^k}{(\Delta x)^2} + O((\Delta x)^2),\end{aligned} \tag{4.34}$$

So we arrive at the explicit scheme:

$$\begin{aligned}\frac{\rho_j^{k+1} - \rho_j^k}{\Delta t} &= \frac{D_\rho}{\lambda_1}\left(\lambda_1 \rho_{xx}^k - 2\sigma_x^k \rho_x^k - \sigma \rho_{xx}^k - \sigma_{xx}^k \rho_j^k\right), \\ &\quad + b_\rho \frac{\lambda_1 - \sigma_j^k}{\lambda_1} \rho_j^k \left(1 - \frac{\rho_j^k}{N}\right) \\ \frac{\nu^{k+1} - \nu^k}{\Delta t} &= D_\nu \nu_{xx}^k + g_1 \frac{(\rho_j^k / \nu_j^k)\tilde{H}_\theta(\sigma_j^k - \sigma_a^*)}{K + (\rho_j^k / \nu_j^k)\tilde{H}_\theta(\sigma_j^k - \sigma_a^*)} \nu_j^k (1 - \nu_j^k), \\ &\quad - g_2 \nu_j^k (\rho_j^k)^n \\ \frac{\sigma_j^{k+1} - \sigma_j^k}{\Delta t} &= D_\sigma \sigma_{xx}^k + h_1 \nu_j^k (\sigma_0 - \sigma_j^k) - h_2 \rho_j^k \sigma_j^k,\end{aligned} \tag{4.35}$$

where we use $p_{xx}^k = \frac{\rho_{j-1}^k - 2\rho_j^k + \rho_{j+1}^k}{(\Delta x)^2} + O((\Delta x)^2)$, and analogously for $\sigma_{xx}^k, \nu_{xx}^k$.

Implementing this scheme caused several overflows in the calculation of the approximation of the Heaviside step function. So we changed the above to include an actual Heaviside function, $H(o_j^k - o_a^*)$, which lead to improved calculations and reasonable results.

4.3 Results

In this section, we summarize the results obtained from the numerical implementation with varying parameters. We discuss the baseline Fisher-Kolmogoroff model for glioma cell density, $\rho(x,t)$, with constant oxygen concentration, $\sigma(x,t) = \sigma_0$, and constant density of functional vasculature, $\nu(x,t) = \nu_0$. As well, we discuss the full model for the interplay of glioma cell density, oxygen concentration and density of functional vasculature.

4.3.1 Fisher-Kolmogoroff Cell Density Model

The baseline Fisher-Kolmogoroff cell density model (FK), outlined in equation (4.22), shows the following characteristics. We distinguish several cases, varying the diffusion rate, D_ρ, and the proliferation rate, b_ρ, of glioma cells.

FK - Case (I)

Case (I) describes the baseline model, taking the parameters as described in table 4.1. The results can be observed in Figure 4.1 and Figure 4.2, respectively Figure A.1 and Figure A.2 of the appendix[2]:

- Local cell density at the origin decreases as the tumour starts to migrate.
- Over time, we see both a proliferation at the site of the origin and further migration. The initial drop in cell density is eventually equalized after close to a year. The tumour grows due to both mechanisms.
- Overall, diffusion rate is still low, the tumour only migrates to a small part of the domain and the proliferation is also rather weak.

[2]The other figures for varying the parameters are included in the appendix to guarantee better readability of the main text.

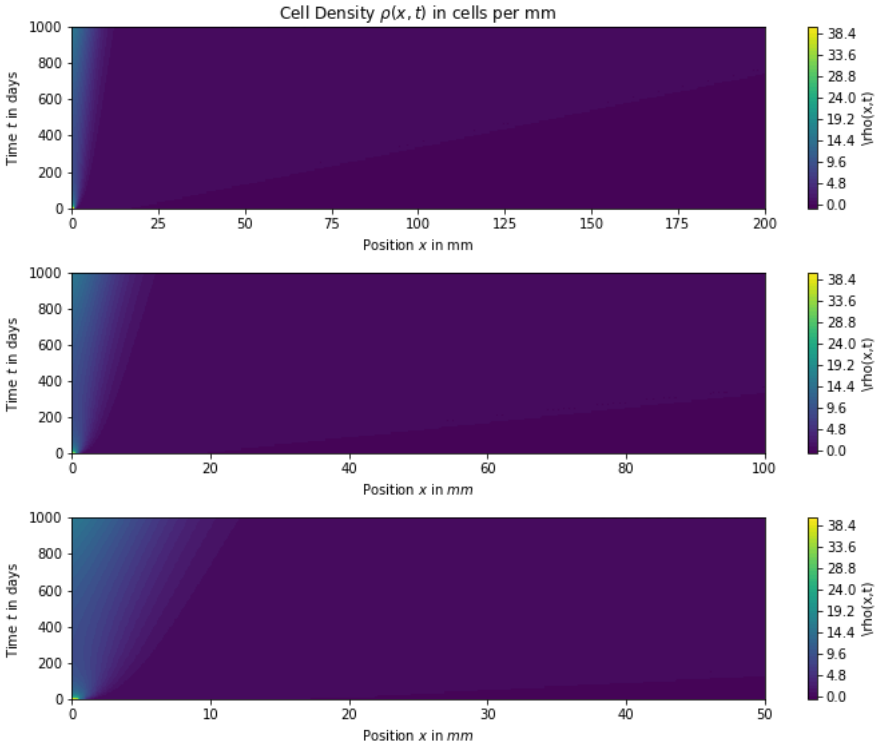

Figure 4.1: Implementation of the basic Fisher-Kolmogoroff model with constant oxygen concentration and vascular density. The figure shows a contour-plot for the evolution of the cell density $\rho(x,t)$ over time and for different resolutions. The parameters are described in table 4.1. We assume the diffusion rate of glioma cells to be $D_\rho = 2.73 \times 10^{-2}\text{mm}^2\text{day}^{-1}$. The proliferation rate of glioma cells is assumed to be $b_\rho = 2.73 \times 10^{-3}\text{mm}^2\text{day}^{-1}$.

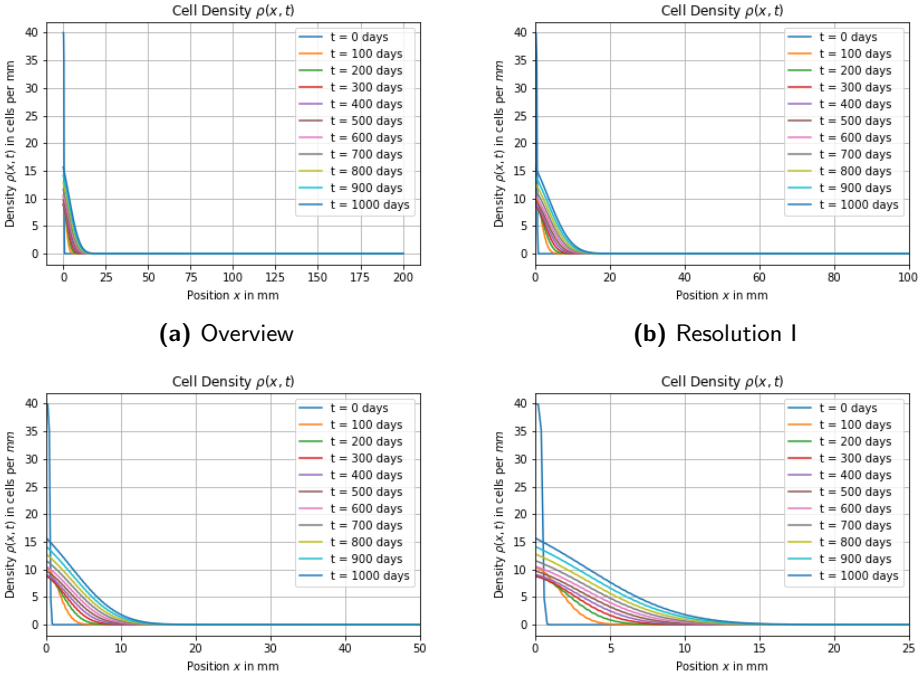

(a) Overview **(b)** Resolution I

(c) Resolution II **(d)** Resolution III

Figure 4.2: Implementation of the basic Fisher-Kolmogoroff model with constant oxygen concentration and vascular density. The figure provides the plot for the basic model. The parameters are described in table 4.1. We assume the diffusion rate of glioma cells to be $D_\rho = 2.73 \times 10^{-2}\text{mm}^2\text{day}^{-1}$. The proliferation rate of glioma cells is assumed to be $b_\rho = 2.73 \times 10^{-3}\text{mm}^2\text{day}^{-1}$. We increase the resolution from figure (a) to (d), showing smaller parts of the domain close to the origin.

FK - Cases (II) - (IV)

In a next step, we increased the diffusion and proliferation rates of glioma cells to the maximum values, $D_\rho = 2.73 \times 10^{-1}\text{mm}^2\text{day}^{-1}$ and $b_\rho = 2.73 \times 10^{-2}\text{mm}^2\text{day}^{-1}$, of the range given in the Alfonso et al. [5] paper. The results are shown in Figure 4.1 and Figure 4.2, for the baseline scenario, in Figure A.3 and Figure A.4, for case (II) with an increased diffusion rate, in Figure A.5 and Figure A.6 for case (III) with an increased proliferation rate. Figure A.7 and Figure A.8 show the results for case (IV) with an increase in both diffusion and proliferation rate.

- Case (II): An increase in the diffusion rate, D_ρ, enables the tumour to spread farther and faster into the brain tissue. As well, we observe an increase in the local growth of the tumour, since this migratory behaviour allows access to more nutrients in the domain. The shape of the curve changes to a an inverse logarithmic shape. Overall, tumours with higher diffusion rates can be characterised as more malignant (c.f. Figure A.3 and Figure A.4).
- Case (III): An increase in the proliferation rate, b_ρ, leads to strong local growth of the tumour. We observe growth beyond the initial tumour cell density and the tumour grows locally until the brain carrying capacity is reached. With this strong proliferation, we also observe the tumour to migrate farther into the brain compared to the base case. The tumour growth shows now an S-shaped pattern. Compared to the case of only increasing the tumour diffusion rate, we observe an even more malignant tumour. The glioma cells do not migrate as far, but proliferation is much more pronounced. Overall, the tumour volume is far larger (c.f. Figure A.5 and Figure A.6).
- Case (IV): Increasing both rates simultaneously leads to the tumour growing faster and farther into the brain tissue and the mechanisms enhance each other. Compared to the previous case, cells start to migrate faster and the proliferation close to the tumour origin is delayed. As in the previous case, the tumour still grows until the brain carrying capacity is reached. Overall, the tumour volume is far larger due to strong local proliferation and migration far into the tissue (c.f. Figure A.7 and Figure A.8).

4.3.2 Interplay Model

Implementing the interplay model (IM), as outlined in the system of equations (4.29), caused several overflows in the calculation of the approximation of the Heaviside step function, $\tilde{H}_\theta(o_j^k - o_a^*)$. So we changed the above to include an actual Heaviside function, $H(o_j^k - o_a^*)$, which lead to improved calculations and reasonable results.

Remark 4.1 *During this process, we encountered some pitfalls and learnings. At first, we tried to stick to the original model, approximating the Heaviside step function with the exponential approach. Encountering overflows and python returning nan-values forced us to search for different packages that allow for large values in the calculations. The 'mpmath' package seemed to be a valid option, but working with this package required iterating over each position in the solution vector individually (c.f. [41]). The program did not compile even after running for hours. Trying to speed up the process with parallel computing via the 'joblib' package did not prove successful either ([1]).*

Then we tried to solve the IVP relying on the 'py-pde' package, which is designed to solve partial differential equations and has extensive examples for biological systems (Zwicker [56]). The package proved useful for implementing the baseline Fisher-Kolmogoroff model. But implementing the approximation of the Heaviside step function caused the system to run into overflows and produced unphysical results. Unfortunately, the package does not provide support for working with a Heaviside step function and so we were again forced to try a different approach. Finally, implementing the actual Heaviside step function via the 'numpy' package produced the results that we are expecting to see from the given model (c.f. [2]).

We distinguish several cases, varying the diffusion rate, D_ρ, and the proliferation rate, b_ρ, of glioma cells, the oxygen consumption rate, h_2, and the vaso-occlusion rate, g_2.

IM - Case (I)

Case (I) describes the baseline model, taking the parameters as described in table 4.1. The results are shown in Figure 4.3 and again in the appendix in Figure B.1. Figure 4.4, and again in the appendix in Figure B.2, shows the results with line plots to describe the evolution over time.[3]

- We observe a slow spread and low growth of the tumour in the brain tissue. The oxygen uptake is limited. The vasculature spreads out farthest and established vasculature persists over time.
- The cell density initially decreases at the origin and the tumour only spreads slightly. Over time, the initial drop in cell density close to the origin is recovered and the tumour grows overall. We understand this in terms of a proliferation at the origin, and migration into the brain tissue, followed by local proliferation at the newly accessed sites.
- The oxygen concentration drops initially and stays almost the same over time. Nonetheless, the oxygen consumption is quite low in this model and oxygen concentration even recovers over time.

[3]The figures for the other cases are included in the appendix to guarantee better readability of the main text.

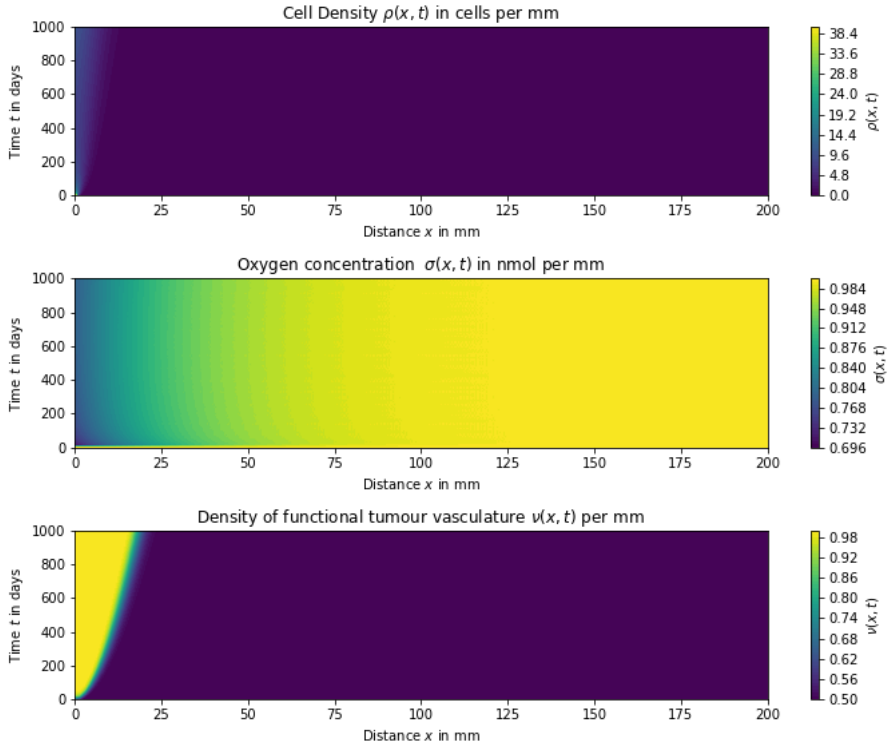

Figure 4.3: Implementation of the interplay model. The figure provides the plot for the interplay model, using the explicit scheme described in equation (4.35). The parameters are described in table 4.1.

- The vasculature reaches outwards and precedes the tumour cells.

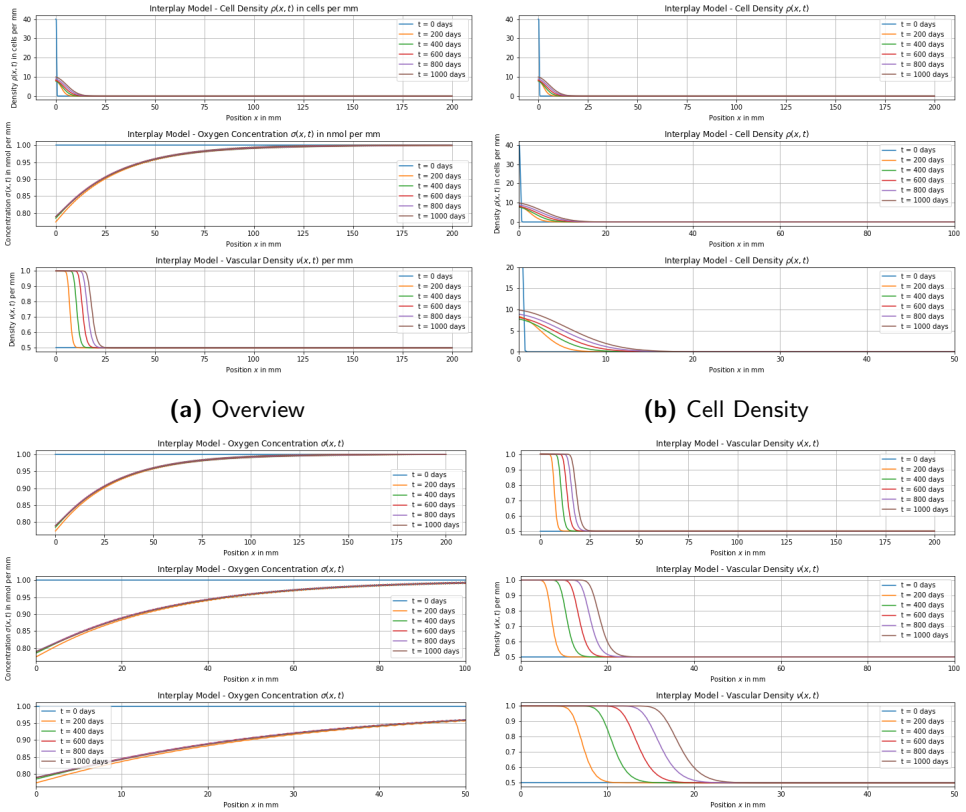

(a) Overview **(b)** Cell Density

(c) Oxygen Concentration **(d)** Vascular Density

Figure 4.4: Implementation of the interplay model. The figure provides the plot for the interplay model, using the explicit scheme described in equation (4.35). The parameters are described in table 4.1. Subfigure (a) shows an overview of the model variables. Subfigures (b), (c), (d) show the cell density, oxygen concentration and the vascular density for different resolutions.

IM - Case (II)

In a next step, we increased the diffusion and proliferation rates of glioma cells, $D_\rho = 2.73 \times 10^{-1}\text{mm}^2\text{day}^{-1}$ and $b_\rho = 2.73 \times 10^{-2}\text{mm}^2\text{day}^{-1}$, the cell oxygen consumption rate, $h_2 = 1.14 \times 10^{-1}\text{mm cell}^{-1}\text{ day}^{-1}$, and the vaso-occlusion rate, $g_2 = 1.5 \times 10^{-11}\text{ cell}^{-6}\text{mm}^{-6}\text{ day}^{-1}$, to the maximum values of the range given in the Alfonso et al. [5] paper. The results are shown in Figure B.3 and Figure B.4.

- We now observe both a strong proliferatory and a strong migratory behaviour, compared to the initial model.
- Compared to the baseline Fisher-Kolmogoroff model, the growth is still limited since we now better account for a depletion of resources in the tissue.
- Oxygen concentration shows an S-shaped form and we can observe the large drop in concentration at the site of the tumour origin.
- The oxygen concentration does not recover anymore and the brain tissue is oxygen depleted. This can be seen in the local concentration at the tumour origin and over large parts of the domain.
- Initially, the vasculature grows locally and then further over the domain. We observe a strong development of vasculature in the brain tissue. Due to the high density of glioma cells close to the tumour origin, vaso-occlusion is distinct. The exerted pressure leads to collapse of adjacent vessels. The density of functional tumour vasculature close to the origin decreases over time.

IM - Case (III)

Here, we want to see the difference to only increasing the cell oxygen consumption rate, h_2, and the vaso-occlusion rate, g_2, while keeping the glioma cell diffusion, D_ρ, and proliferation rates, b_ρ, at their initial level. The results are shown in Figure B.5 and Figure B.6.

- The proliferatory and migratory behaviour of the tumour is not pronounced. The cell density close to the tumour origin decreases and the tumour spreads into a small part of the nearby brain tissue.
- The oxygen concentration follows a similar pattern to the initial case, but now the oxygen concentration does not recover over time.
- The vascular density is minimally affected by the change in parameters. The tumour growth is small compared to the case of higher diffusion, D_ρ, and proliferation rates, b_ρ, and the tumour does not suppress functional tumour vasculature, since the brain carrying capacity is not reached.

IM - Case (IV)

In Case (IV) we compare these results to only increasing the diffusion, D_ρ, and proliferation rate, b_ρ, of glioma cells, but keeping the cell oxygen consumption rate, h_2, and the vaso-occlusion rate,g_2, at the initial level. The results are shown in Figure B.7 and Figure B.8.

- The development of the glioma cell density is comparable to the second case of the Fisher-Kolmogoroff model and we observe a more distinct proliferation. The tumour spreads faster and farther into the tissue.
- Since the tumour shows higher growth rates, more oxygen is required to fuel this growth and the oxygen concentration is lower compared to the base case. Now, oxygen levels do not recover in the observed timeframe. Oxygen depletion in the brain can be observed.
- The spread of the vasculature precedes the spread of the tumour. But since the tumour cell density is higher overall, we observe a decrease of the vascular density at the origin. Over time, the vascular density collapses under the pressure exerted by the growing tumour. Vaso-occlusion is distinct. At some parts of the domain, the glioma cell density reaches the brain carrying capacity and the vasculature is obliterated.

IM - Case (V)

Now, we want to analyse the behaviour for only increasing either the oxygen consumption rate, h_2, or the vaso-occlusion rate, g_2. The model shows more distinct behaviours when the diffusion, D_ρ, and proliferation rates, b_ρ, of glioma cells are increased and so we use this as the new baseline for our comparison. The results for increasing the oxygen consumption rate, h_2, are shown in Figure B.9 and Figure B.10.

- Higher demand for oxygen significantly limits cell proliferation.
- Infiltration of the tumour into the domain stays the same, but the tumour size is less distinct and tumour cell density is lower overall.
- Due to the lower proliferation, vaso-occlusion is not observed.
- Oxygen concentration is significantly lower and tissue at the location of the tumour is oxygen depleted.

IM - Case (VI)

As well, we analyse the results for only increasing the vaso-occlusion rate, g_2, for the new base case of higher diffusion and proliferation rates. The results are shown in Figure B.11 and Figure B.12.

- The vasculature spreads as far into the tissue as in the base case.
- Vaso-occlusion is more distinct. Occlusion occurs faster and at a larger size of the domain. Again, the vascular density collapses under the pressure exerted by the growing tumour. Vaso-occlusion is distinct. At the parts of the domain close to the tumour origin, the glioma cell density reaches the brain carrying capacity and the vasculature is obliterated.
- Cell density and oxygen concentration are not affected by the change in parameters.

Chapter 5

Discussion and Outlook

5.1 Discussion

In this thesis, we focused on reaction-diffusion models in the context of brain tumours, analysing the migration-proliferation model of Alfonso et al. [5] for the behaviour of glioma cells. At first, we provided a short overview regarding the biology of tumours and gliomas. We explained the hallmarks of cancer to provide a basic understanding and gave an overview of the properties of gliomas. In particular, we described behaviour, function, and structure of gliomas, that cause them to resist treatment and lead to their increased survival and growth rates. We finished this part by outlining the model assumptions for the Alfonso et al. [5] migration-proliferation model, embedding their assumptions in the biological context. In the next part, we provided a theoretical overview regarding reaction-diffusion equations and analysed the particular example of the Fisher-Kolmogoroff equation. We explained that balance laws form the basis for reaction-diffusion systems and showed how the diffusion equation can be derived from a simple random walk approach. The last chapter described the migration-proliferation dichotomy following the work of Alfonso et al. [5]. We replicated the model and provided a numerical analysis, confirming parts of the results of the authors.

The model uses an extended version of the Fisher-Kolmogoroff equation to describe the interplay of glioma cell density, oxygen concentration and density of functional tumour vasculature. We implemented the baseline Fisher-Kolmogoroff model for glioma cell density and the full model for the interplay of glioma cell density, oxygen concentration and density of functional tumour vasculature. Analysing the models, we focused on the effects of changing the diffusion, D_ρ, and proliferation, b_ρ, rates of glioma cell density. In the interplay model, we additionally vary the vaso-occlusion rate, g_2, and the oxygen consumption rate, h_2. Overall, we find that increasing the diffusion

rate, D_ρ, and the proliferation rate, b_ρ, to the maximum values of the provided range proved to be most significant in both models. The effects enhance each other via the following mechanism: Higher proliferation requires more nutrients, here accounted for in terms of oxygen, at the respective location to support local growth. But the fast paced growth depletes the region of oxygen, creating a hypoxic environment and thus forcing the tumour to migrate. While spreading over the domain, the tumour shows a strong growth at the newly accessed sites, which are still sufficiently rich in oxygen. Thus, the process continues. This results in the tumour to show a really malignant behaviour. The tumour grows more distinct at the site of the origin and spreads faster and farther into the brain tissue, depleting the tissue of oxygen. Also a denser network of functional vasculature is created to prepare the ground for the tumour to spread into the domain. The tumour growth then starts to occupy the brain tissue, until the brain carrying capacity is reached. In this process, existing vasculature collapses under the growing tumour. The tumour dominates the area.

We can observe the migration-proliferation dichotomy of glioma cells. A strong proliferation of glioma cells can be seen for an oxygen concentration of $\sigma(x,t) > \frac{\sigma_0}{2}\sigma_0 = 0.5$ nmol mm^{-1}. Below this value, the proliferation weakens significantly and the migration behaviour of glioma cells becomes more distinct. This becomes even more pronounced when the oxygen concentration drops below the threshold for hypoxia, $\sigma(x,t) < \frac{\sigma_0}{4} = 0.25$ nmol mm^{-1}. Whereas the tumour shows a strong proliferative behaviour in a normoxic environment, the migratory behaviour is more distinct the less oxygen is available at a given location. The ability to switch phenotypes supports the overall tumour growth, which we can observe in the interplay model 4.3.2. The model confirms the migration-proliferation dichotomy of glioma cells.

The effects of increasing the vaso-occlusion rate, g_2, are observed in cases of distinct growth of the glioma cells. As outlined above, the growing tumour starts to occupy the brain tissue, thereby suppressing existing vasculature. In the case of a higher vaso-occlusion rate, g_2, this process is more distinct and vasculature collapses at a faster pace. We do not observe significant changes in the proliferative or migratory behaviour of glioma cells, which slightly diverges from the findings of Alfonso et al. [5].

Increasing the oxygen consumption rate, h_2, significantly limits the proliferation of the tumour. The process can be understood as follows. More oxygen is required to fuel the proliferation of glioma cells. This hinders growth since the brain tissue becomes oxygen depleted at a faster rate and the environment turns hypoxic. The overall growth is restricted and the malignancy of the tumour decreases. In line with the findings of Alfonso et al. [5], we observe gliomas to be less proliferative.

The findings indicate different approaches for therapy. Limiting the oxygen

availability for glioma cells significantly decreases tumour growth in the whole domain and has the potential to limit the malignancy of a given tumour. But this might come at the cost of the tumour showing a slightly more pronounced migratory behaviour. Spreading farther into the brain tissue might increase the level of difficulty to eradicate the tumour in total. Glioma cells evolve in the tissue by growing vasculature to access nutrients at other sites. Removing vasculature might present an option to hinder tumour growth and restrict the tumour to the occupied locations.

5.2 Outlook

The migration-proliferation dichotomy is a truly fascinating case of one of the many mechanisms that tumour cells posses to survive and grow. Given the scope of this thesis, we can only analyse selected aspects of this mechanism, of the mathematical models trying to describe the behaviour and of the underlying math. We want to use this section to discuss aspects that can be analysed and implemented in subsequent works.

Glioma cells switch phenotypes to adapt to their surroundings. Referencing the works of Godlewski et al. [17] and Höring et al. [25], Alfonso et al. [5] assume this switching process between a migratory and a proliferatory phenotype (c.f. equation (4.2)) to be linear. Other works model the phenotype switching process to be nonlinear and put more focus on the tumour environment. For example, Heidary et al. [23] analyse the interactions between fibroblasts, a component of the tumour microenvironment, and cancer cells. In particular, they rely on a nonlinear agent-based model to describe the various intracellular reactions between cancer cells and fibroblasts and the intercellular interactions to explain the duality of fibroblasts acting as supporters and inhibitors of cancer growth. Zhang et al. [54] model how the epidermal growth factor receptor gene-protein interaction influences the phenotype. Subsequent works can analyse whether a linear process fits best to available data and account more for the role of the cell environment. According to Godlweski et al. [17], micro-RNAs, a certain class of gene expression regulators, can have a significant influence on the pathway. Especially, miR-451 is found to regulate the proliferation and migration mechanism, while according to Zhao et al. [55] proteins, precisely tripartite motif-containing (TRIM) family proteins, such as TRIM21 are also found to have a non-negligible influence. According to the works of Godlewski et al. [17], Kuznetsov et al. [30], or Zhang et al. [54], the glucose levels in the environment are shown to influence the go-or-grow mechanism as well. This motivates to extend the model at hand in order to account for the mentioned aspects.

Other variations of the model are found in the works of Mascheroni et

al. [36, 37]. The authors [36] highlight nutrient and mechanical stress factors that influence the migration-proliferation dichotomy. Walker et al. [52] show that the influence of mechanical stresses on tumour growth is significant. So accounting for morphoelasticity, combining solid mechanics and growth, in subsequent models will further improve this work.

This also leads us to the following: In the work of Alfonso et al. [5] and in this thesis, only a one-dimensional version of the model is discussed and implemented. This motivates an implementation of the scheme in two or three dimensions which then allows to better capture the effects of morphoelasticity and provides a more realistic picture (c.f. Hubbard and Byrne [24], Pham et al. [47] or Walker et al. [52]). A two- or three-dimensional model also allows to account for the differences between white and grey matter of the brain tissue. Following the work of Swanson et al. [49], the diffusion rate of gliomas change significantly in these different environments.

In a different paper, Mascheroni et al. [37] rely on a similar system of PDEs to model the glioma cell density and oxygen concentration. Compared to the model of Alfonso et al. [5], the density of functional vasculature is modeled in a slightly simpler version, which does not account for the pro-angiogenic factor production, consumption and natural decay in the same level of detail. Their model is used to predict therapeutic outcomes. They combine this model with a machine learning approach and achieve results in accordance with clinical outcomes. This validates both versions of the system of PDEs and motivates the step towards using the models to predict therapeutic outcomes and treatment strategies.

In this thesis, we implement only one simplified version of the Alfonso et al. [5] model. We restrict ourselves to work with a migratory to proliferative phenotypic switching parameter of $\lambda_2 = 1$. So we obtain

$$\alpha(\sigma) = \frac{\lambda_1 - \sigma}{(\lambda_2 - 1)\sigma + \lambda_1} = \frac{\lambda_1 - \sigma}{\lambda_1} \quad \text{and} \quad \beta(\sigma) = \frac{\lambda_2 \sigma}{(\lambda_2 - 1)\sigma + \lambda_1} = \frac{\sigma}{\lambda_1}.$$

This simplifies the diffusion term in equation (4.8), now only relying on the oxygen concentration in the numerator, and hence the overall equation for the tumour cell density $\rho(x, t)$. Alfonso et al. [5] describe that increasing the tumour front speed increases with larger values for λ_2, while the infiltration width decreases. So slight quantitative changes in the behaviour of glioma cells are observed, but overall the model shows that the behaviour of glioma cells is preserved. Nonetheless, implementing the model for different values for the migratory to proliferative phenotypic switching parameter will provide additional value in subsequent works.

As well, reviewing the existing literature regarding the range of values for the different parameters (compare table 4.1) can provide value by either verifying or updating the model simulations.

Another point regards the numerical analysis. The implementation can be updated in terms of compilation time which then allows to better compare the outcomes for different input values. Trying different solvers and different numerical schemes can be done in subsequent works.

Following up on this work by implementing some of the suggestions will improve the model and can contribute to more insights into the migration-proliferation dichotomy of glioma cells. Better understanding this mechanism and verifying the model with clinical data should improve treatment strategies and allow to better predict clinical outcomes. Extending the model to account for various treatment options, so for example by removing existing vasculature or limiting oxygen supply, will improve this model and contribute to improve treatment strategies.

Remark 5.1 *Here, I want to conclude by giving a brief summary of the learnings along the way and provide a short personal outlook. This thesis allowed me to step on the field of biomathematics. It provided an opportunity to learn about the biology of cancer and glioma cells, to dive into the field of partial differential equations and to apply and extend my skillset from numerical analysis. It refreshed and improved my coding skills and motivates me to further improve my analytical and numerical skills. Continuing to work on cancer modelling sparks my interest and deems to be a field for which I want to invest more time and effort to properly understand the biology and mathematical parts involved. This field has the means to provide value for patients and the models need verification with patient data. This is an additional motivation to dive into statistics to provide another perspective on the field.*

Bibliography

[1] *Joblib: running Python functions as pipeline jobs — joblib 1.4.2 documentation*.

[2] *NumPy reference — NumPy v1.26 Manual*.

[3] Bhavesh K. Ahir, Herbert H. Engelhard, and Sajani S. Lakka, *Tumor Development and Angiogenesis in Adult Brain Tumor: Glioblastoma*, Molecular Neurobiology **57** (2020), no. 5, 2461–2478 (en).

[4] Ali Ahmed, Muhammad Uzair UlHaq, Zartasha Mustansar, Arslan Shaukat, and Lee Margetts, *How growing tumour impacts intracranial pressure and deformation mechanics of brain*, Royal Society Open Science (2021) (en).

[5] J. C. L. Alfonso, A. Köhn-Luque, T. Stylianopoulos, F. Feuerhake, A. Deutsch, and H. Hatzikirou, *Why one-size-fits-all vaso-modulatory interventions fail to control glioma invasion: in silico insights*, Scientific Reports **6** (2016), no. 1, 37283 (en), Publisher: Nature Publishing Group.

[6] Joshua Adam Bull and Helen Mary Byrne, *The Hallmarks of Mathematical Oncology*, Proceedings of the IEEE **110** (2022), no. 5, 523–540, Conference Name: Proceedings of the IEEE.

[7] K. Böttger, H. Hatzikirou, A. Chauviere, and A. Deutsch, *Investigation of the Migration/Proliferation Dichotomy and its Impact on Avascular Glioma Invasion*, Mathematical Modelling of Natural Phenomena **7** (2012), no. 1, 105–135 (en).

[8] Katrin Böttger, Haralambos Hatzikirou, Anja Voss-Böhme, Elisabetta Ada Cavalcanti-Adam, Miguel A. Herrero, and Andreas Deutsch, *An Emerging Allee Effect Is Critical for Tumor Initiation and Persistence*, PLOS Computational Biology **11** (2015), no. 9, e1004366 (en).

[9] Robert Stephen Cantrell and Chris Cosner, *Spatial Ecology via Reaction-Diffusion Equations*, John Wiley & Sons, January 2004 (en).

[10] Peter Carmeliet and Rakesh K. Jain, *Principles and mechanisms of vessel normalization for cancer and other angiogenic diseases*, Nature Reviews Drug Discovery **10** (2011), no. 6, 417–427 (en).

[11] Lawrence C. Evans, *Partial Differential Equations*, American Mathematical Society, March 2022 (en), Google-Books-ID: Ott1EAAAQBAJ.

[12] R. A. Fisher, *The Wave of Advance of Advantageous Genes*, Annals of Eugenics **7** (1937), no. 4, 355–369 (en), _eprint: https://onlinelibrary.wiley.com/doi/pdf/10.1111/j.1469-1809.1937.tb02153.x.

[13] Gautier Follain, David Herrmann, Sébastien Harlepp, Vincent Hyenne, Naël Osmani, Sean C. Warren, Paul Timpson, and Jacky G. Goetz, *Fluids and their mechanics in tumour transit: shaping metastasis*, Nature Reviews Cancer **20** (2020), no. 2, 107–124 (en), Publisher: Nature Publishing Group.

[14] Chong-Feng Gao, Qian Xie, Yan-Li Su, Julie Koeman, Sok Kean Khoo, Margaret Gustafson, Beatrice S. Knudsen, Rick Hay, Nariyoshi Shinomiya, and George F. Vande Woude, *Proliferation and invasion: Plasticity in tumor cells*, Proceedings of the National Academy of Sciences **102** (2005), no. 30, 10528–10533, Publisher: Proceedings of the National Academy of Sciences.

[15] C. Giaume, F. Kirchhoff, C. Matute, A. Reichenbach, and A. Verkhratsky, *Glia: the fulcrum of brain diseases*, Cell Death & Differentiation **14** (2007), no. 7, 1324–1335 (en), Publisher: Nature Publishing Group.

[16] A. Giese, R. Bjerkvig, M.E. Berens, and M. Westphal, *Cost of Migration: Invasion of Malignant Gliomas and Implications for Treatment*, Journal of Clinical Oncology **21** (2003), no. 8, 1624–1636 (en).

[17] Jakub Godlewski, Agnieszka Bronisz, Michal O. Nowicki, E. Antonio Chiocca, and Sean Lawler, *microRNA-451: A conditional switch controlling glioma cell proliferation and migration*, Cell Cycle **9** (2010), no. 14, 2814–2820 (en).

[18] Peter Grindrod, *Patterns And Waves: The Theory and Application of Reaction-Diffusion Equations*, April 2021.

[19] Magdalena Götz, *Biology and Function of Glial Cells*, Neurosciences - From Molecule to Behavior: a university textbook (C. Giovanni Galizia and

Pierre-Marie Lledo, eds.), Springer, Berlin, Heidelberg, 2013, pp. 163–177 (en).

[20] Douglas Hanahan, *Hallmarks of Cancer: New Dimensions*, Cancer Discovery **12** (2022), no. 1, 31–46 (en).

[21] Douglas Hanahan and Robert A Weinberg, *The Hallmarks of Cancer*, Cell **100** (2000), no. 1, 57–70 (en).

[22] Douglas Hanahan and Robert A. Weinberg, *Hallmarks of Cancer: The Next Generation*, Cell **144** (2011), no. 5, 646–674 (en).

[23] Zarifeh Heidary, Jafar Ghaisari, Shiva Moein, and Shaghayegh Haghjooy Javanmard, *The double-edged sword role of fibroblasts in the interaction with cancer cells; an agent-based modeling approach*, PLOS ONE **15** (2020), no. 5, e0232965 (en).

[24] M. E. Hubbard and H. M. Byrne, *Multiphase modelling of vascular tumour growth in two spatial dimensions*, Journal of Theoretical Biology **316** (2013), 70–89.

[25] Elisabeth Höring, Patrick Nikolaus Harter, Janina Seznec, Jens Schittenhelm, Hans-Jörg Bühring, Shohag Bhattacharyya, Elke von Hattingen, Cornelia Zachskorn, Michel Mittelbronn, and Ulrike Naumann, *The "go or grow" potential of gliomas is linked to the neuropeptide processing enzyme carboxypeptidase E and mediated by metabolic stress*, Acta Neuropathologica **124** (2012), no. 1, 83–97 (en).

[26] Rakesh K. Jain, Emmanuelle di Tomaso, Dan G. Duda, Jay S. Loeffler, A. Gregory Sorensen, and Tracy T. Batchelor, *Angiogenesis in brain tumours*, Nature Reviews Neuroscience **8** (2007), no. 8, 610–622 (en), Publisher: Nature Publishing Group.

[27] Rakesh K. Jain, John D. Martin, and Triantafyllos Stylianopoulos, *The Role of Mechanical Forces in Tumor Growth and Therapy*, Annual Review of Biomedical Engineering **16** (2014), no. Volume 16, 2014, 321–346 (en), Publisher: Annual Reviews.

[28] Kristjan R Jessen, *Glial cells*, The International Journal of Biochemistry & Cell Biology **36** (2004), no. 10, 1861–1867.

[29] A Kolmogoroff, *Étude de l'équation de la diffusion avec croissance de la quantité de matière et son application à un problème biologigue*, Moscow Univ. Bull. Ser. Internat. Sect. A **1** (1937), 1.

[30] M. Kuznetsov, J. Clairambault, and V. Volpert, *Improving cancer treatments via dynamical biophysical models*, Physics of Life Reviews **39** (2021), 1–48.

[31] King-Yeung Lam and Yuan Lou, *Introduction to Reaction-Diffusion Equations: Theory and Applications to Spatial Ecology and Evolutionary Biology*, Springer Nature, December 2022 (en), Google-Books-ID: QnKfEAAAQBAJ.

[32] Andrew B. Lassman, *Molecular biology of gliomas*, Current Neurology and Neuroscience Reports **4** (2004), no. 3, 228–233 (en).

[33] David N. Louis, Hiroko Ohgaki, Otmar D. Wiestler, and Webster K. Cavenee (eds.), *WHO Classification of Tumours of the Central Nervous System*, revised 4th edition ed., WHO Classification of tumours series, International Agency for Research on Cancer, Lyon, 2016 (en).

[34] Roberta Lugano, Mohanraj Ramachandran, and Anna Dimberg, *Tumor angiogenesis: causes, consequences, challenges and opportunities*, Cellular and Molecular Life Sciences **77** (2020), no. 9, 1745–1770 (en).

[35] Cicely K. Macnamara, *Biomechanical modelling of cancer: Agent-based force-based models of solid tumours within the context of the tumour microenvironment*, Computational and Systems Oncology **1** (2021), no. 2, e1018 (en), _eprint: https://onlinelibrary.wiley.com/doi/pdf/10.1002/cso2.1018.

[36] Pietro Mascheroni, Juan Carlos López Alfonso, Maria Kalli, Triantafyllos Stylianopoulos, Michael Meyer-Hermann, and Haralampos Hatzikirou, *On the Impact of Chemo-Mechanically Induced Phenotypic Transitions in Gliomas*, Cancers **11** (2019), no. 5, 716 (en), Number: 5 Publisher: Multidisciplinary Digital Publishing Institute.

[37] Pietro Mascheroni, Symeon Savvopoulos, Juan Carlos López Alfonso, Michael Meyer-Hermann, and Haralampos Hatzikirou, *Improving personalized tumor growth predictions using a Bayesian combination of mechanistic modeling and machine learning*, Communications Medicine **1** (2021), no. 1, 1–14 (en), Publisher: Nature Publishing Group.

[38] Andrew Massey, Jamie Stewart, Chynna Smith, Cameron Parvini, Moira McCormick, Kun Do, and Alexander X. Cartagena-Rivera, *Mechanical properties of human tumour tissues and their implications for cancer development*, Nature Reviews Physics **6** (2024), no. 4, 269–282 (en), Publisher: Nature Publishing Group.

[39] S R McKeown, *Defining normoxia, physoxia and hypoxia in tumours—implications for treatment response*, The British Journal of Radiology **87** (2014), no. 1035, 20130676.

[40] Denis Mollison, *Spatial Contact Models for Ecological and Epidemic Spread*, Journal of the Royal Statistical Society. Series B (Methodological) **39** (1977), no. 3, 283–326, Publisher: [Royal Statistical Society, Wiley].

[41] The mpmath development team, *mpmath: a {P}ython library for arbitrary-precision floating-point arithmetic (version 1.3.0)*, 2023.

[42] J.D. Murray (ed.), *Mathematical Biology, I. An Introduction*, 3 ed., Interdisciplinary Applied Mathematics, Springer New York, NY, 2002.

[43] WHO Classification of Tumours Editorial Board, *Central Nervous System Tumours*, 5th edition ed., WHO Classification of tumours series, vol. 6, International Agency for Research on Cancer, Lyon, 2021 (en).

[44] Akira Okubo and Simon A. Levin, *Diffusion and Ecological Problems: Modern Perspectives*, Interdisciplinary Applied Mathematics, vol. 14, Springer New York, NY, 2001.

[45] OpenAI, *ChatGPT (GPT-4)*, 2024.

[46] Timothy P. Padera, Brian R. Stoll, Jessica B. Tooredman, Diane Capen, Emmanuelle di Tomaso, and Rakesh K. Jain, *Cancer cells compress intratumour vessels*, Nature **427** (2004), no. 6976, 695–695 (en), Publisher: Nature Publishing Group.

[47] Kara Pham, Arnaud Chauviere, Haralambos Hatzikirou, Xiangrong Li, Helen M. Byrne, Vittorio Cristini, and John Lowengrub, *Density-dependent quiescence in glioma invasion: instability in a simple reaction–diffusion model for the migration/proliferation dichotomy*, Journal of Biological Dynamics **6** (2012), no. sup1, 54–71, Publisher: Taylor & Francis _eprint: https://doi.org/10.1080/17513758.2011.590610.

[48] Birthe Krogh Rasmussen, Steinbjørn Hansen, René J. Laursen, Michael Kosteljanetz, Henrik Schultz, Bente Mertz Nørgård, Rikke Guldberg, and Kim Oren Gradel, *Epidemiology of glioma: clinical characteristics, symptoms, and predictors of glioma patients grade I–IV in the the Danish Neuro-Oncology Registry*, Journal of Neuro-Oncology **135** (2017), no. 3, 571–579 (en).

[49] K. R. Swanson, E. C. Alvord Jr, and J. D. Murray, *A quantitative model for differential motility of gliomas in grey and white matter*, Cell Proliferation **33** (2000), no. 5, 317–329 (en), _eprint: https://onlinelibrary.wiley.com/doi/pdf/10.1046/j.1365-2184.2000.00177.x.

[50] Kristin R. Swanson, Russell C. Rockne, Jonathan Claridge, Mark A. Chaplain, Ellsworth C. Alvord, and Alexander R.A. Anderson, *Quantifying the Role of Angiogenesis in Malignant Progression of Gliomas: In Silico Modeling Integrates Imaging and Histology*, Cancer Research **71** (2011), no. 24, 7366–7375 (en).

[51] Pauli Virtanen, Ralf Gommers, Travis E. Oliphant, Matt Haberland, Tyler Reddy, David Cournapeau, Evgeni Burovski, Pearu Peterson, Warren Weckesser, Jonathan Bright, Stéfan J. Van Der Walt, Matthew Brett, Joshua Wilson, K. Jarrod Millman, Nikolay Mayorov, Andrew R. J. Nelson, Eric Jones, Robert Kern, Eric Larson, C J Carey, İlhan Polat, Yu Feng, Eric W. Moore, Jake VanderPlas, Denis Laxalde, Josef Perktold, Robert Cimrman, Ian Henriksen, E. A. Quintero, Charles R. Harris, Anne M. Archibald, Antônio H. Ribeiro, Fabian Pedregosa, Paul Van Mulbregt, SciPy 1.0 Contributors, Aditya Vijaykumar, Alessandro Pietro Bardelli, Alex Rothberg, Andreas Hilboll, Andreas Kloeckner, Anthony Scopatz, Antony Lee, Ariel Rokem, C. Nathan Woods, Chad Fulton, Charles Masson, Christian Häggström, Clark Fitzgerald, David A. Nicholson, David R. Hagen, Dmitrii V. Pasechnik, Emanuele Olivetti, Eric Martin, Eric Wieser, Fabrice Silva, Felix Lenders, Florian Wilhelm, G. Young, Gavin A. Price, Gert-Ludwig Ingold, Gregory E. Allen, Gregory R. Lee, Hervé Audren, Irvin Probst, Jörg P. Dietrich, Jacob Silterra, James T Webber, Janko Slavič, Joel Nothman, Johannes Buchner, Johannes Kulick, Johannes L. Schönberger, José Vinícius De Miranda Cardoso, Joscha Reimer, Joseph Harrington, Juan Luis Cano Rodríguez, Juan Nunez-Iglesias, Justin Kuczynski, Kevin Tritz, Martin Thoma, Matthew Newville, Matthias Kümmerer, Maximilian Bolingbroke, Michael Tartre, Mikhail Pak, Nathaniel J. Smith, Nikolai Nowaczyk, Nikolay Shebanov, Oleksandr Pavlyk, Per A. Brodtkorb, Perry Lee, Robert T. McGibbon, Roman Feldbauer, Sam Lewis, Sam Tygier, Scott Sievert, Sebastiano Vigna, Stefan Peterson, Surhud More, Tadeusz Pudlik, Takuya Oshima, Thomas J. Pingel, Thomas P. Robitaille, Thomas Spura, Thouis R. Jones, Tim Cera, Tim Leslie, Tiziano Zito, Tom Krauss, Utkarsh Upadhyay, Yaroslav O. Halchenko, and Yoshiki Vázquez-Baeza, *SciPy 1.0: fundamental algorithms for scientific computing in Python*, Nature Methods **17** (2020), no. 3, 261–272 (en).

[52] Benjamin J. Walker, Giulia L. Celora, Alain Goriely, Derek E. Moulton, and Helen M. Byrne, *Minimal Morphoelastic Models of Solid Tumour Spheroids: A Tutorial*, Bulletin of Mathematical Biology **85** (2023), no. 5, 38 (en).

[53] Manfred Westphal and Katrin Lamszus, *The neurobiology of gliomas: from cell biology to the development of therapeutic approaches*, Nature Reviews Neuroscience **12** (2011), no. 9, 495–508 (en).

[54] Le Zhang, Chaitanya A. Athale, and Thomas S. Deisboeck, *Development of a three-dimensional multiscale agent-based tumor model: Simulating gene-protein interaction profiles, cell phenotypes and multicellular patterns in brain cancer*, Journal of Theoretical Biology **244** (2007), no. 1, 96–107.

[55] Zhipeng Zhao, Yuqi Wang, Dapeng Yun, Qilin Huang, Delong Meng, Qing Li, Pingzhao Zhang, Chenji Wang, Hongyan Chen, and Daru Lu, *TRIM21 overexpression promotes tumor progression by regulating cell proliferation, cell migration and cell senescence in human glioma*, American Journal of Cancer Research **10** (2020), no. 1, 114–130.

[56] David Zwicker, *py-pde: A Python package for solving partial differential equations*, Journal of Open Source Software **5** (2020), no. 48, 2158 (en).

Appendix A

Fisher-Kolmogoroff Cell Density Model

Here we show the plots obtained from the numerical implementation of the mathematical model as described in chapter 4. In this part, we show the plots for the baseline Fisher-Kolmogoroff model (FK) for the glioma cell density, assuming constant oxygen concentration, $\sigma(x,t) = \sigma_0$, and constant density of functional vasculature, $\nu(x,t) = \nu_0$. The parameters are described in table 4.1. We distinguish several cases, varying the diffusion rate, D_ρ, and the proliferation rate, b_ρ, of glioma cells:

- Case (I A) describes the baseline model.
- Case (II A) describes the outcomes for increasing the diffusion rate, D_ρ. The proliferation rate of glioma cells, b_ρ, stays unchanged.
- Case (III A) describes the outcomes for increasing the proliferation rate, b_ρ, of glioma cells. The diffusion rate, D_ρ, stays at the baseline level.
- Case (IV A) describes the outcomes for increasing the diffusion rate, D_ρ, and the proliferation rate, b_ρ, of glioma cells.

FK - Case I

Case I describes the baseline model. The parameters are described in table 4.1.

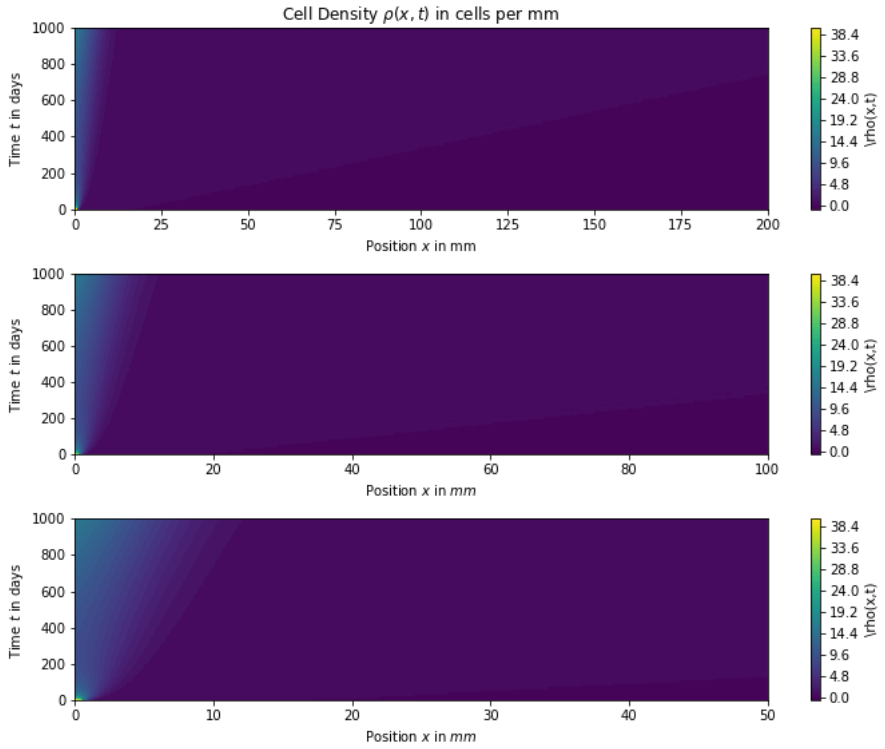

Figure A.1: Implementation of the basic Fisher-Kolmogoroff model with constant oxygen concentration and vascular density. The figure shows a contour-plot for the evolution of the cell density $\rho(x,t)$ over time and for different resolutions. The parameters are described in table 4.1. We assume the diffusion rate of glioma cells to be $D_\rho = 2.73 \times 10^{-2}\text{mm}^2\text{day}^{-1}$. The proliferation rate of glioma cells is assumed to be $b_\rho = 2.73 \times 10^{-3}\text{mm}^2\text{day}^{-1}$.

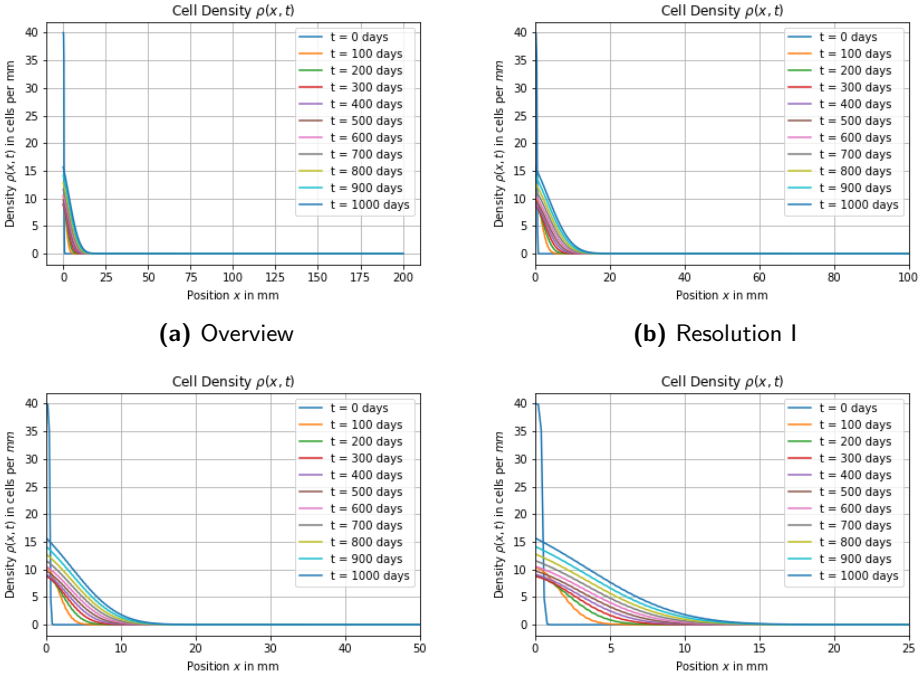

(a) Overview **(b)** Resolution I

(c) Resolution II **(d)** Resolution III

Figure A.2: Implementation of the basic Fisher-Kolmogoroff model with constant oxygen concentration and vascular density. The figure provides the plot for the basic model. The parameters are described in table 4.1. We assume the diffusion rate of glioma cells to be $D_\rho = 2.73 \times 10^{-2}\text{mm}^2\text{day}^{-1}$. The proliferation rate of glioma cells is assumed to be $b_\rho = 2.73 \times 10^{-3}\text{mm}^2\text{day}^{-1}$. We increase the resolution from figure (a) to (d), showing smaller parts of the domain close to the origin.

FK - Case II

Here, the diffusion rate of glioma cells is $D_p = 2.73 \times 10^{-1}\text{mm}^2$ per day. The proliferation rate, b_ρ, of glioma cells stays unchanged.

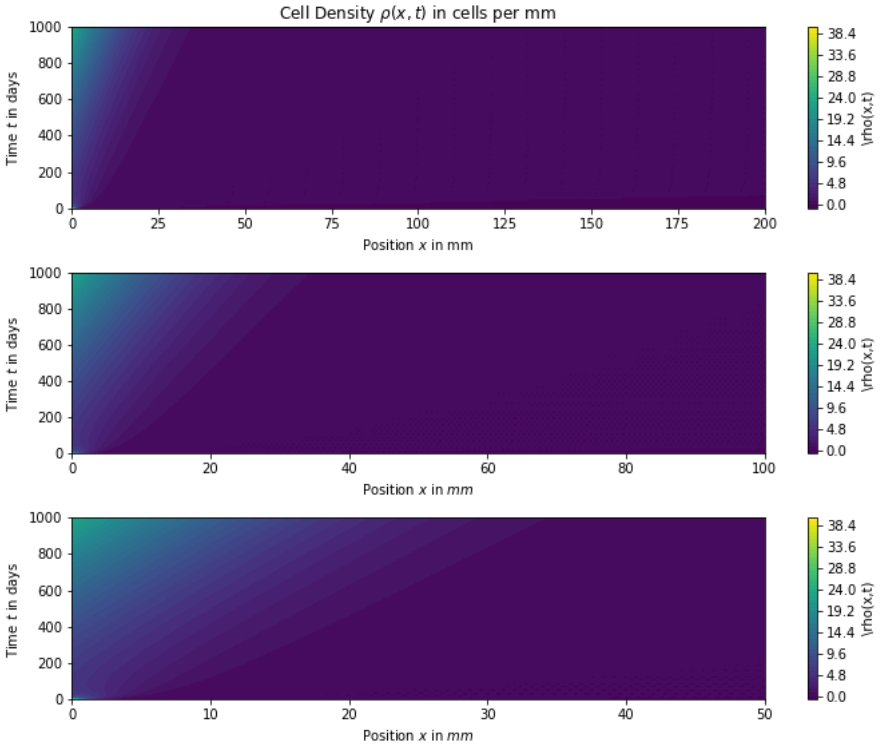

Figure A.3: Implementation of the basic Fisher-Kolmogoroff model with constant oxygen concentration and vascular density. The figure shows a contour-plot for the evolution of the cell density $\rho(x,t)$ over time and for different resolutions. The parameters are described in table 4.1. Here, the diffusion rate of glioma cells is $D_p = 2.73 \times 10^{-1}\text{mm}^2$ per day. The proliferation rate, b_ρ, of glioma cells stays unchanged.

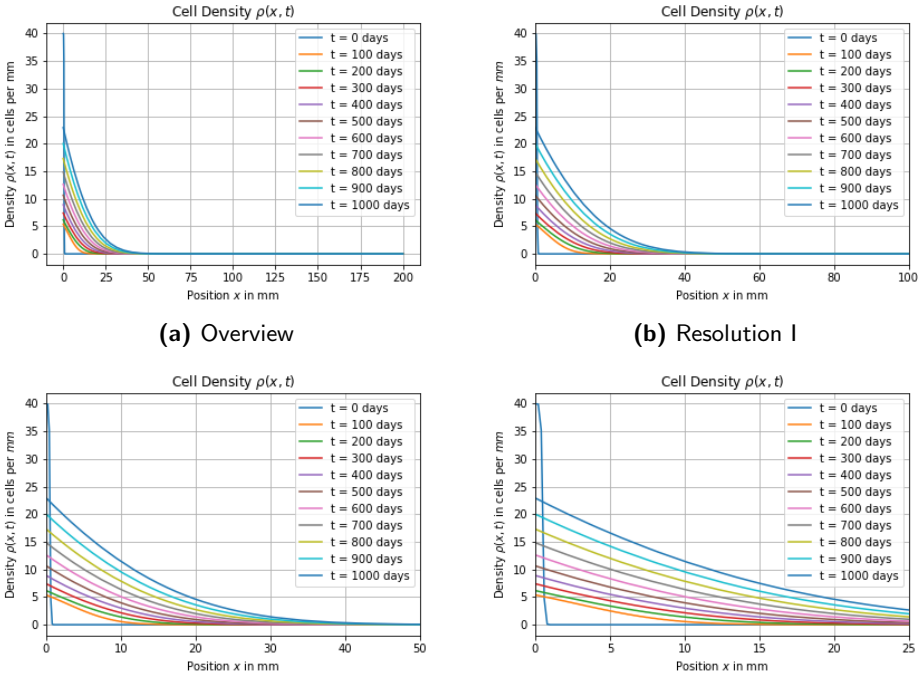

(a) Overview **(b)** Resolution I

(c) Resolution II **(d)** Resolution III

Figure A.4: Implementation of the basic Fisher-Kolmogoroff model with constant oxygen concentration and vascular density. The figure provides the plot for the basic model. The figure on the right shows a version for a smaller length of the domain. The parameters are described in table 4.1. We assume a diffusion rate of glioma cells of $D_p = 2.73 \times 10^{-1}\text{mm}^2$ per day. The proliferation rate of glioma cells, b_ρ, stays unchanged. We increase the resolution from figure (a) to (d), showing smaller parts of the domain close to the origin.

FK - Case III

Here, the proliferation rate of glioma cells is $b_p = 2.73 \times 10^{-2}$ per day. The diffusion rate, D_ρ, of glioma cells stays unchanged.

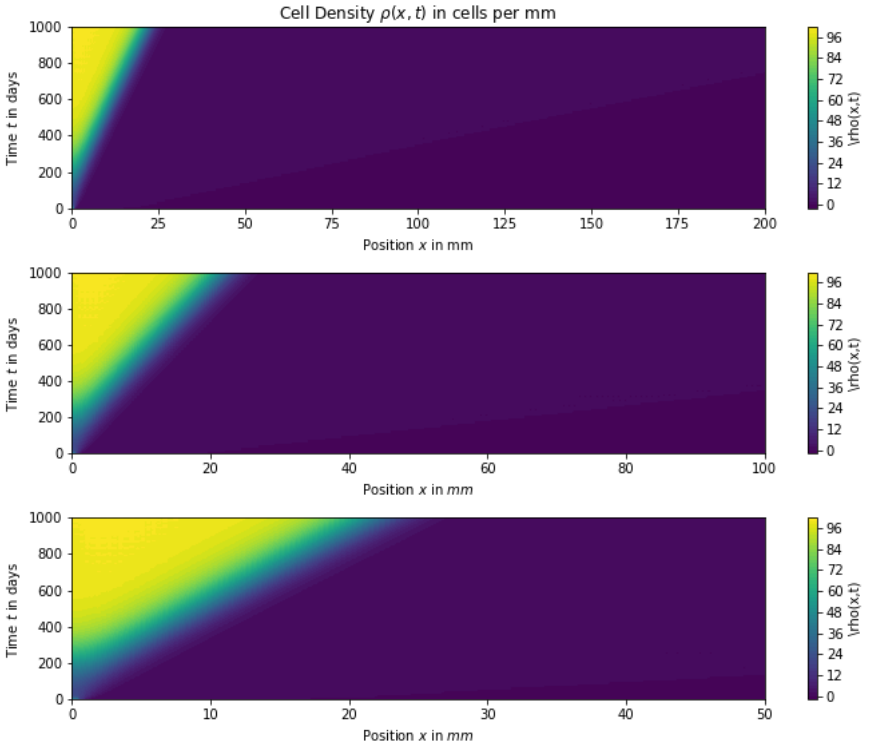

Figure A.5: Implementation of the basic Fisher-Kolmogoroff model with constant oxygen concentration and vascular density. The figure shows a contour-plot for the evolution of the cell density $\rho(x,t)$ over time and for different resolutions. The parameters are described in table 4.1. Here, the proliferation rate of glioma cells is $b_p = 2.73 \times 10^{-2}$ per day. The diffusion rate, D_ρ, of glioma cells stays unchanged.

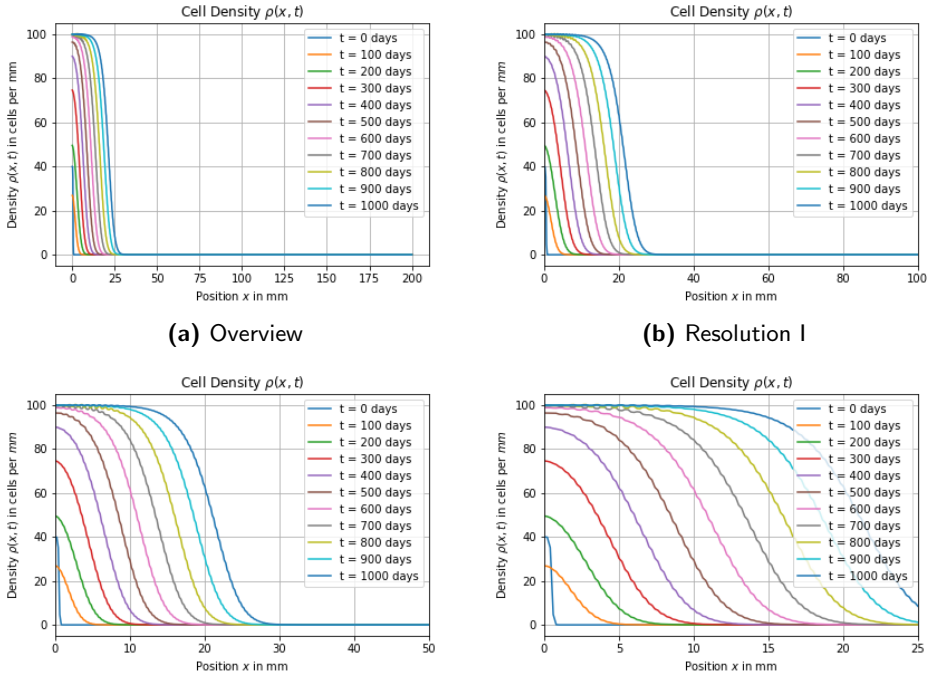

(a) Overview **(b)** Resolution I

(c) Resolution II **(d)** Resolution III

Figure A.6: Implementation of the basic Fisher-Kolmogoroff model with constant oxygen concentration and vascular density. The figure provides the plot for the basic model. The parameters are described in table 4.1. We assume a proliferation rate of glioma cells of $b_p = 2.73 \times 10^{-2}$ per day. The diffusion rate of glioma cells, D_ρ, stays unchanged. We increase the resolution from figure (a) to (d), showing smaller parts of the domain close to the origin.

FK - Case IV

We assume a diffusion rate of glioma cells of $D_p = 2.73 \times 10^{-1}\text{mm}^2$ per day. The proliferation rate of glioma cells is $b_p = 2.73 \times 10^{-2}$ per day.

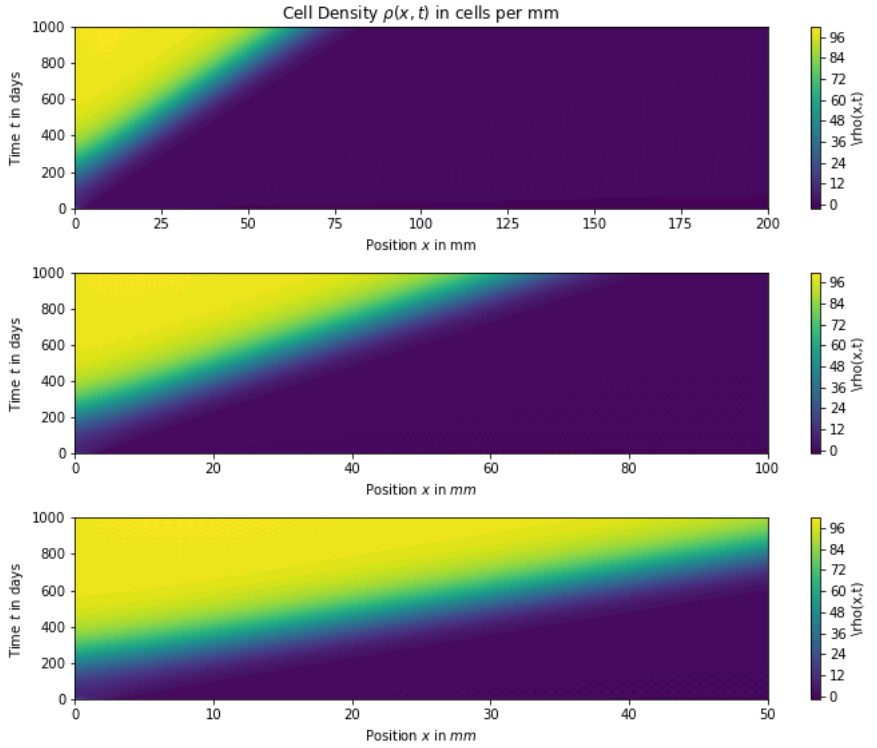

Figure A.7: Implementation of the basic Fisher-Kolmogoroff model with constant oxygen concentration and vascular density. The figure shows a contour-plot for the evolution of the cell density $\rho(x,t)$ over time and for different resolutions. The parameters are described in table 4.1. We assume a diffusion rate of glioma cells of $D_p = 2.73 \times 10^{-1}\text{mm}^2$ per day. The proliferation rate of glioma cells is $b_p = 2.73 \times 10^{-2}$ per day.

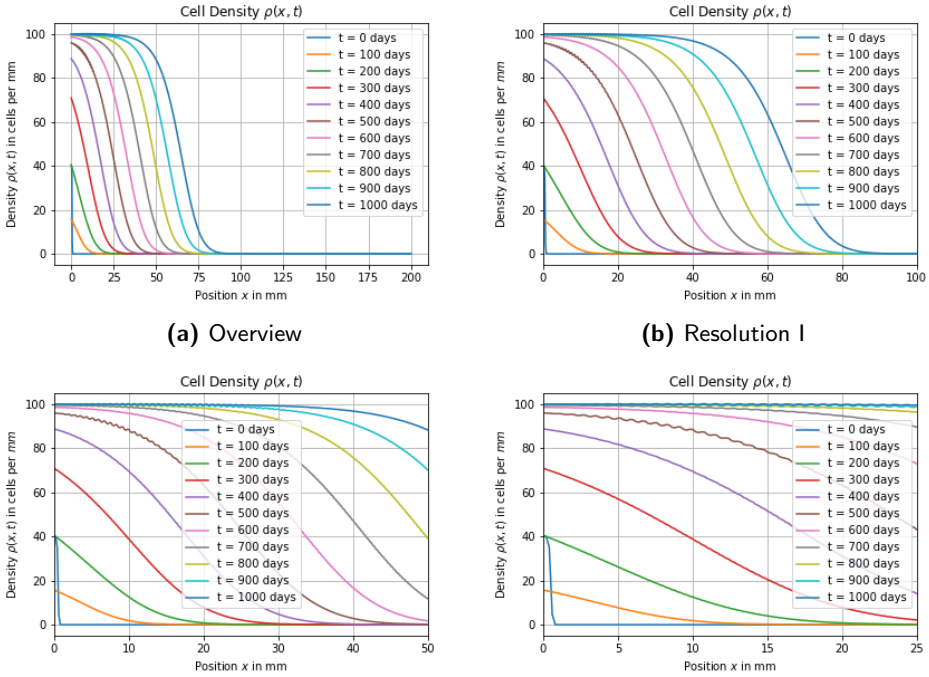

(a) Overview **(b)** Resolution I

(c) Resolution II **(d)** Resolution III

Figure A.8: Implementation of the basic Fisher-Kolmogoroff model with constant oxygen concentration and vascular density. The figure provides the plot for the basic model. The parameters are described in table 4.1. We assume a diffusion rate of glioma cells of $D_p = 2.73 \times 10^{-1}\text{mm}^2$ per day. The proliferation rate of glioma cells is $b_p = 2.73 \times 10^{-2}$ per day. We increase the resolution from figure (a) to (d), showing smaller parts of the domain close to the origin.

Appendix B

Interplay Model

Here we show the plots obtained from the numerical implementation of the mathematical model as described in chapter 4. In this part, we show the plots for the interplay model (IM), the full model for the glioma cell density, oxygen concentration and density of functional vasculature. The parameters are described in table 4.1. We distinguish several cases, varying the diffusion rate, D_ρ, and the proliferation rate, b_ρ, of glioma cells, the oxygen consumption rate, h_2, and the vaso-occlusion rate.

- Case (I B) describes the baseline model.
- Case (II B) describes the outcomes for increasing the diffusion rate, D_ρ, and the proliferation rate, b_ρ, of glioma cells, the oxygen consumption rate, h_2, and the vaso-occlusion rate.
- Case (III B) describes the outcomes for increasing the oxygen consumption rate, h_2, and the vaso-occlusion rate.
- Case (IV B) describes the outcomes for increasing the diffusion rate, D_ρ, and the proliferation rate, b_ρ, of glioma cells.
- Case (V B) describes the outcomes for increasing the diffusion rate, D_ρ, and the proliferation rate, b_ρ, of glioma cells, and increasing the oxygen consumption rate, h_2.
- Case (VI B) describes the outcomes for increasing the diffusion rate, D_ρ, and the proliferation rate, b_ρ, of glioma cells, and increasing the vaso-occlusion rate.

IM - Case (I)

Case I describes the baseline model. The parameters are described in table 4.1.

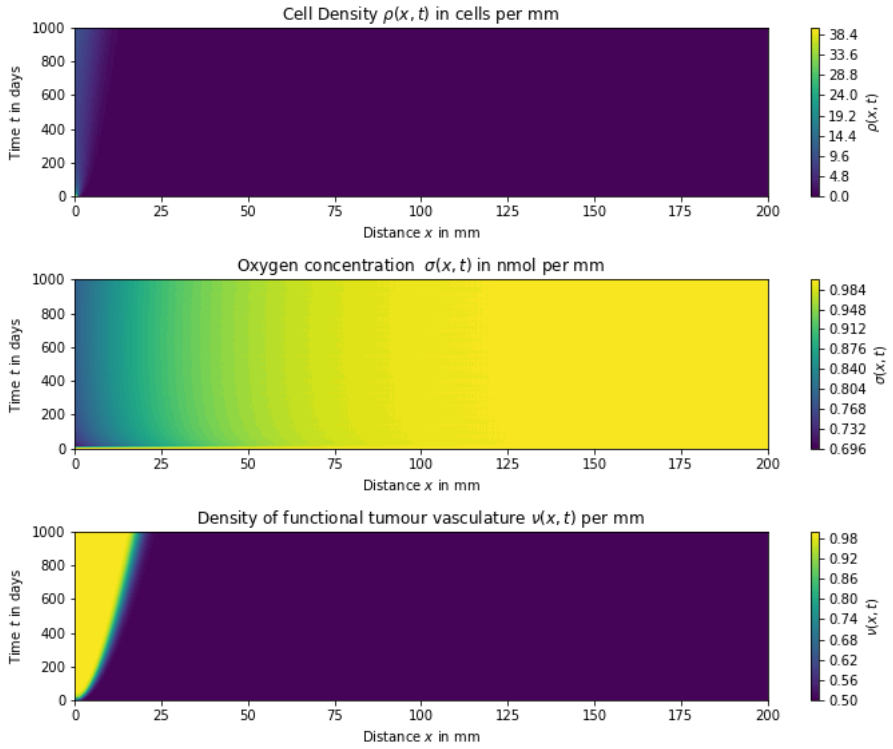

Figure B.1: Implementation of the interplay model. The figure provides the plot for the interplay model, using the explicit scheme described in equation (4.35). The parameters are described in table 4.1.

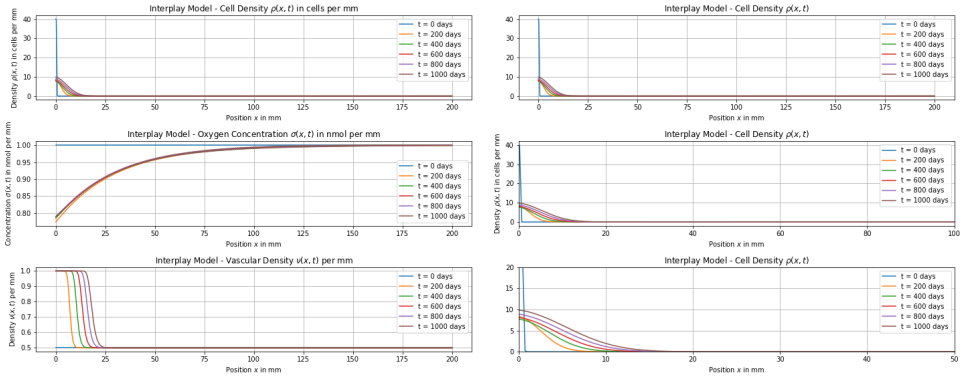

(a) Overview **(b)** Cell Density

(c) Oxygen Concentration **(d)** Vascular Density

Figure B.2: Implementation of the interplay model. The figure provides the plot for the interplay model, using the explicit scheme described in equation (4.35). The parameters are described in table 4.1. Subfigure (a) shows an overview of the model variables. Subfigures (b), (c), (d) show the cell density, oxygen concentration and the vascular density for different resolutions.

IM - Case (II)

Here, we assume a diffusion rate of glioma cells of $D_\rho = 2.73 \times 10^{-1}\text{mm}^2$ per day, a proliferation rate of glioma cells of $b_\rho = 2.73 \times 10^{-2}$ per day, an oxygen consumption rate of $h_2 = 1.14 \times 10^{-1}\text{mm}$ per cell per day and a vaso-occlusion rate of $g_2 = 1.5 \times 10^{-11}$ cell^{-6}mm^{-6} per day.

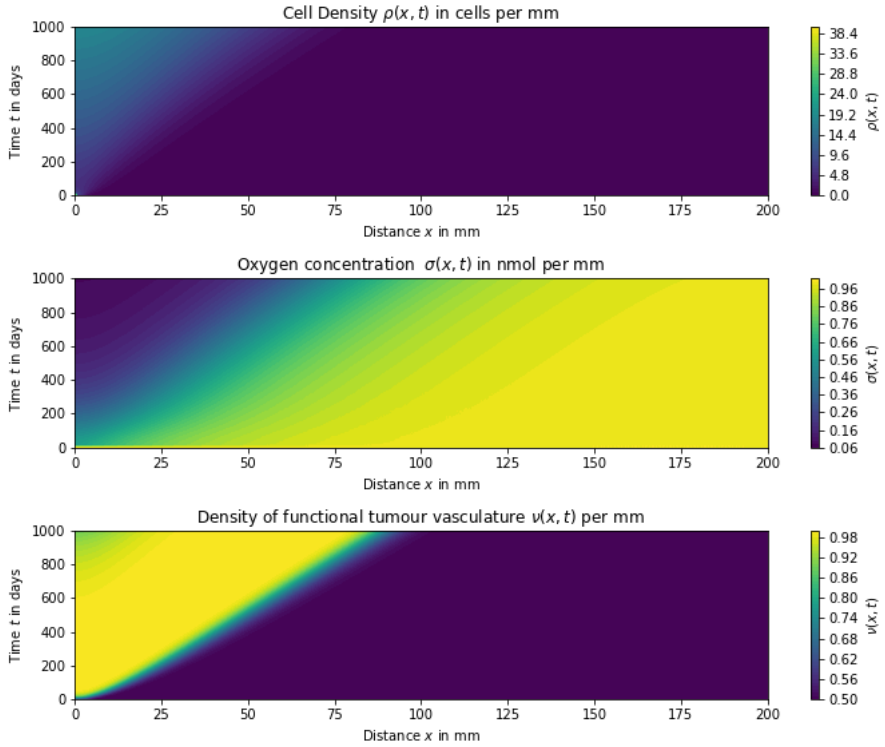

Figure B.3: Implementation of the interplay model. The figure provides the plot for the interplay model, using the explicit scheme described in equation (4.35). The parameters are described in table 4.1. Here, we assume a diffusion rate of glioma cells of $D_\rho = 2.73 \times 10^{-1}\text{mm}^2$ per day, a proliferation rate of glioma cells of $b_\rho = 2.73 \times 10^{-2}$ per day, an oxygen consumption rate of $h_2 = 1.14 \times 10^{-1}\text{mm}$ per cell per day and a vaso-occlusion rate of $g_2 = 1.5 \times 10^{-11}$ cell^{-6}mm^{-6} per day.

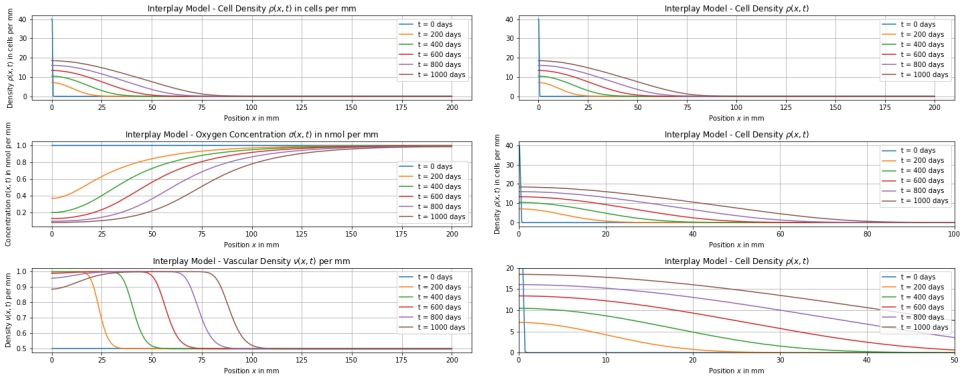

(a) Overview

(b) Cell Density

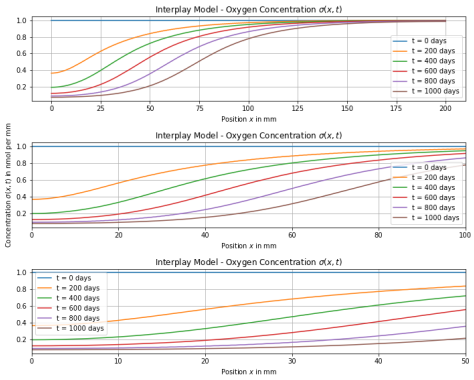

(c) Oxygen Concentration

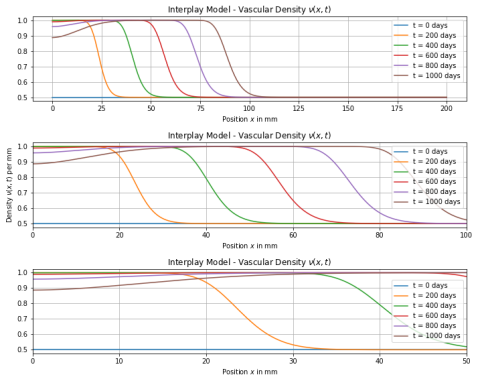

(d) Vascular Density

Figure B.4: Implementation of the interplay model. The figure provides the plot for the interplay model, using the explicit scheme described in equation (4.35). The parameters are described in table 4.1. Here, we assume a diffusion rate of glioma cells of $D_\rho = 2.73 \times 10^{-1}\text{mm}^2$ per day, a proliferation rate of glioma cells of $b_\rho = 2.73 \times 10^{-2}$ per day, an oxygen consumption rate of $h_2 = 1.14 \times 10^{-1}\text{mm}$ per cell per day and a vaso-occlusion rate of $g_2 = 1.5 \times 10^{-11}$ cell^{-6}mm^{-6} per day. Subfigure (a) shows an overview of the model variables. Subfigures (b), (c), (d) show the cell density, oxygen concentration and the vascular density for different resolutions.

IM - Case (III)

Here, we assume an oxygen consumption rate of $h_2 = 1.14 \times 10^{-1}$mm per cell per day and a vaso-occlusion rate of $g_2 = 1.5 \times 10^{-11}$ cell^{-6}mm^{-6} per day. The diffusion rate of glioma cells, D_ρ, and the proliferation rate of glioma cells of b_ρ, stay at the baseline level.

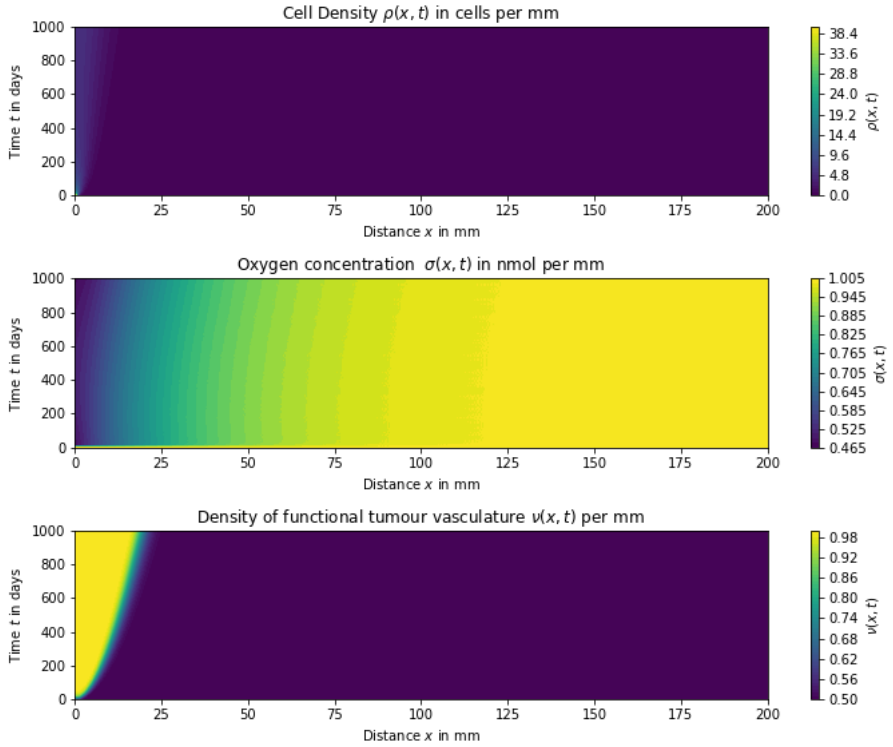

Figure B.5: Implementation of the interplay model. The figure provides the plot for the interplay model, using the explicit scheme described in equation (4.35). The parameters are described in table 4.1. Here, we assume an oxygen consumption rate of $h_2 = 1.14 \times 10^{-1}$mm per cell per day and a vaso-occlusion rate of $g_2 = 1.5 \times 10^{-11}$ cell^{-6}mm^{-6} per day.

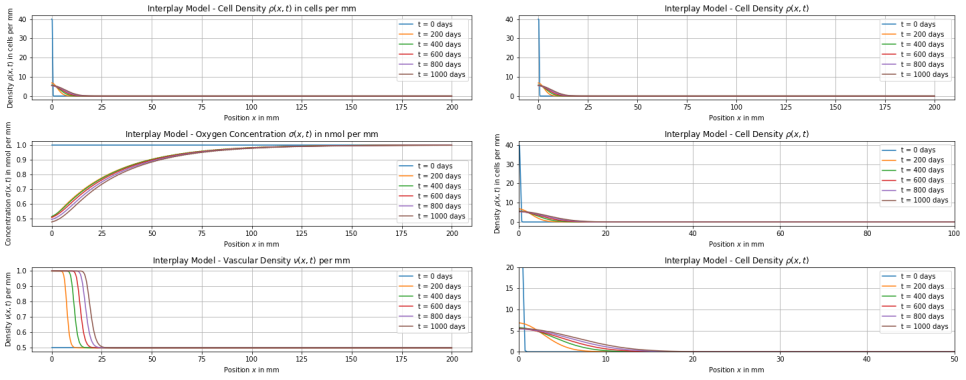

(a) Overview

(b) Cell Density

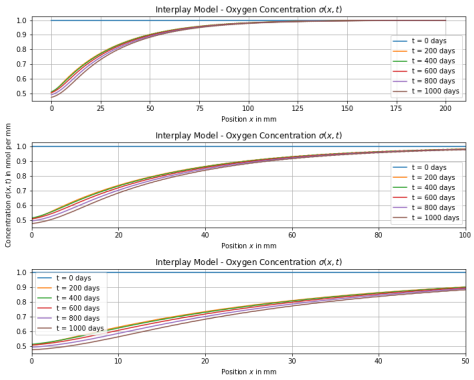

(c) Oxygen Concentration

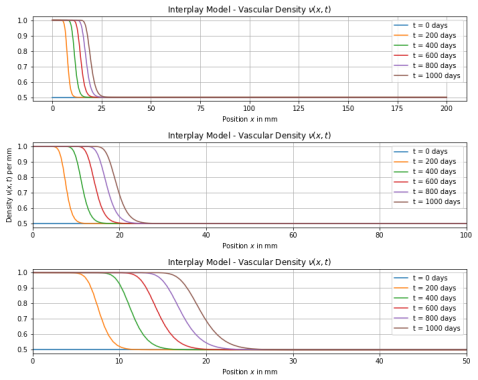

(d) Vascular Density

Figure B.6: Implementation of the interplay model. The figure provides the plot for the interplay model, using the explicit scheme described in equation (4.35). The parameters are described in table 4.1. Here, we assume an oxygen consumption rate of $h_2 = 1.14 \times 10^{-1}$mm per cell per day and a vaso-occlusion rate of $g_2 = 1.5 \times 10^{-11}$ cell^{-6}mm^{-6} per day. Subfigure (a) shows an overview of the model variables. Subfigures (b), (c), (d) show the cell density, oxygen concentration and the vascular density for different resolutions.

IM - Case (IV)

Here, we assume a diffusion rate of glioma cells of $D_\rho = 2.73 \times 10^{-1}\text{mm}^2$ per day, and a proliferation rate of glioma cells of $b_\rho = 2.73 \times 10^{-2}$ per day. The oxygen consumption rate, h_2, and the vaso-occlusion rate, g_2, stay at the baseline level.

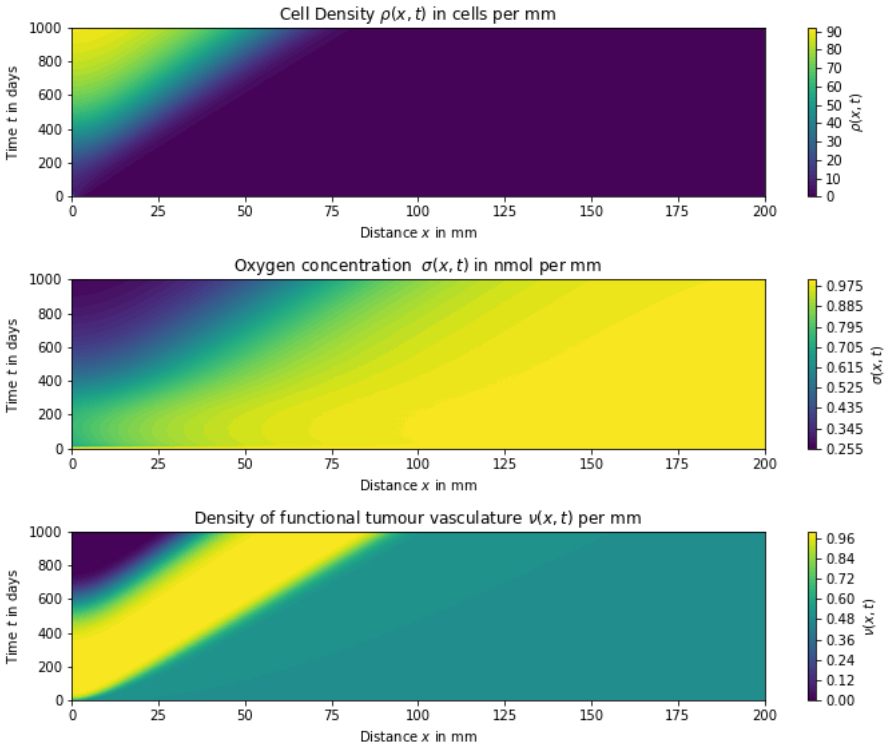

Figure B.7: Implementation of the interplay model. The figure provides the plot for the interplay model, using the explicit scheme described in equation (4.35). The parameters are described in table 4.1. Here, we assume a diffusion rate of glioma cells of $D_\rho = 2.73 \times 10^{-1}\text{mm}^2$ per day, and a proliferation rate of glioma cells of $b_\rho = 2.73 \times 10^{-2}$ per day.

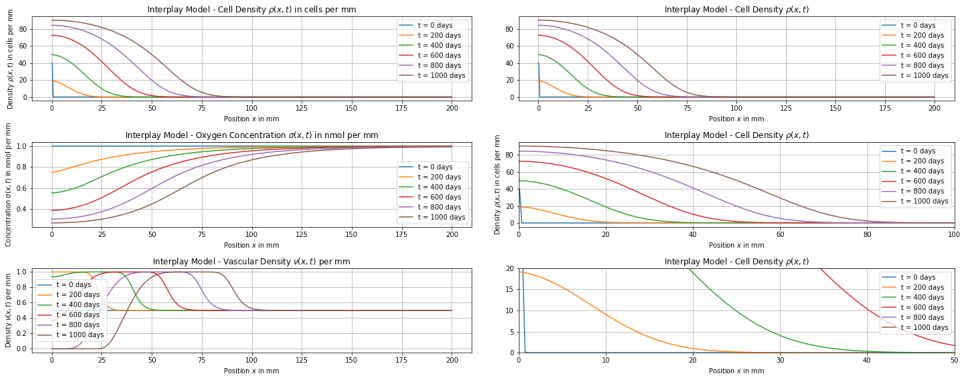

(a) Overview **(b)** Cell Density

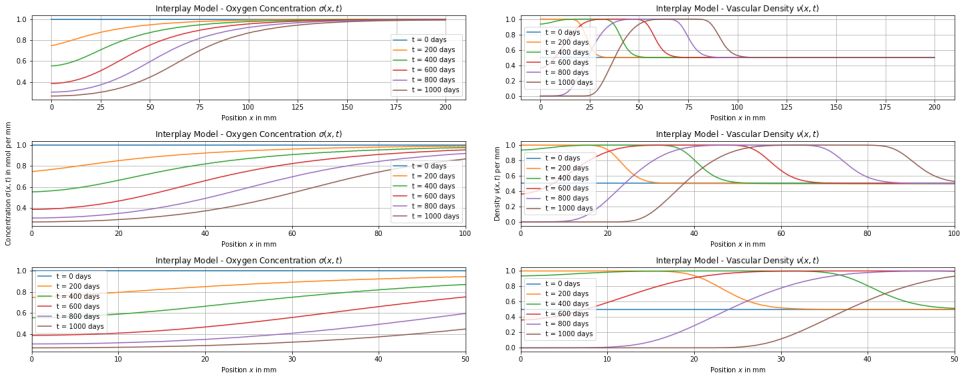

(c) Oxygen Concentration **(d)** Vascular Density

Figure B.8: Implementation of the interplay model. The figure provides the plot for the interplay model, using the explicit scheme described in equation (4.35). The parameters are described in table 4.1. Here, we assume a diffusion rate of glioma cells of $D_\rho = 2.73 \times 10^{-1}\text{mm}^2$ per day, and a proliferation rate of glioma cells of $b_\rho = 2.73 \times 10^{-2}$ per day. Subfigure (a) shows an overview of the model variables. Subfigures (b), (c), (d) show the cell density, oxygen concentration and the vascular density for different resolutions.

IM - Case (V)

Here, we assume a diffusion rate of glioma cells of $D_\rho = 2.73 \times 10^{-1}\text{mm}^2$ per day, a proliferation rate of glioma cells of $b_\rho = 2.73 \times 10^{-2}$ per day, and an oxygen consumption rate of $h_2 = 1.14 \times 10^{-1}\text{mm}$ per cell per day. The vaso-occlusion rate, g_2, stays at the baseline level.

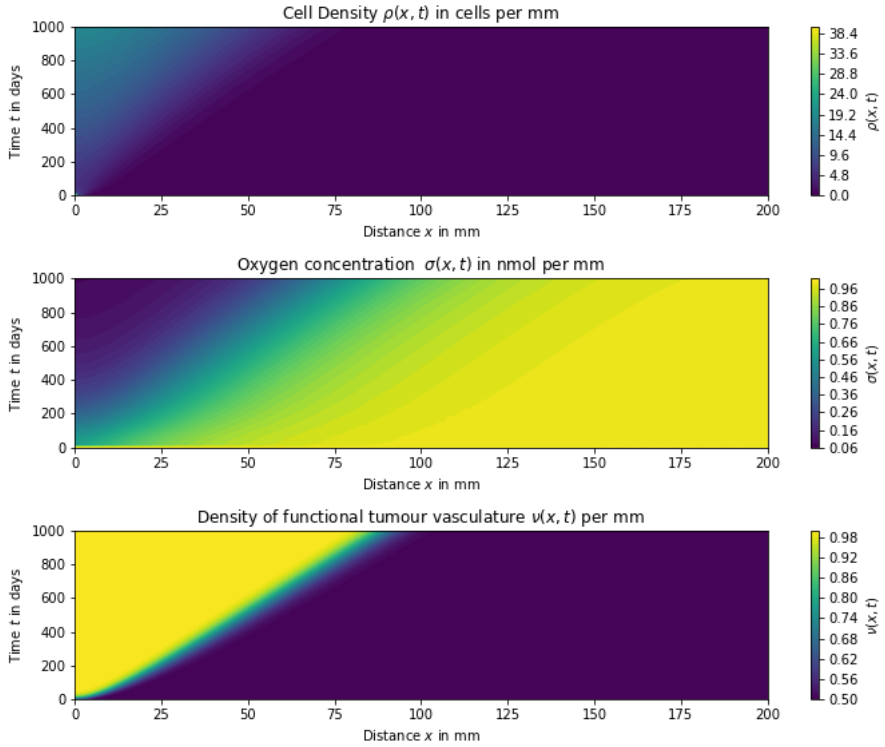

Figure B.9: Implementation of the interplay model. The figure provides the plot for the interplay model, using the explicit scheme described in equation (4.35). The parameters are described in table 4.1. Here, we assume a diffusion rate of glioma cells of $D_\rho = 2.73 \times 10^{-1}\text{mm}^2$ per day, a proliferation rate of glioma cells of $b_\rho = 2.73 \times 10^{-2}$ per day, and an oxygen consumption rate of $h_2 = 1.14 \times 10^{-1}\text{mm}$ per cell per day.

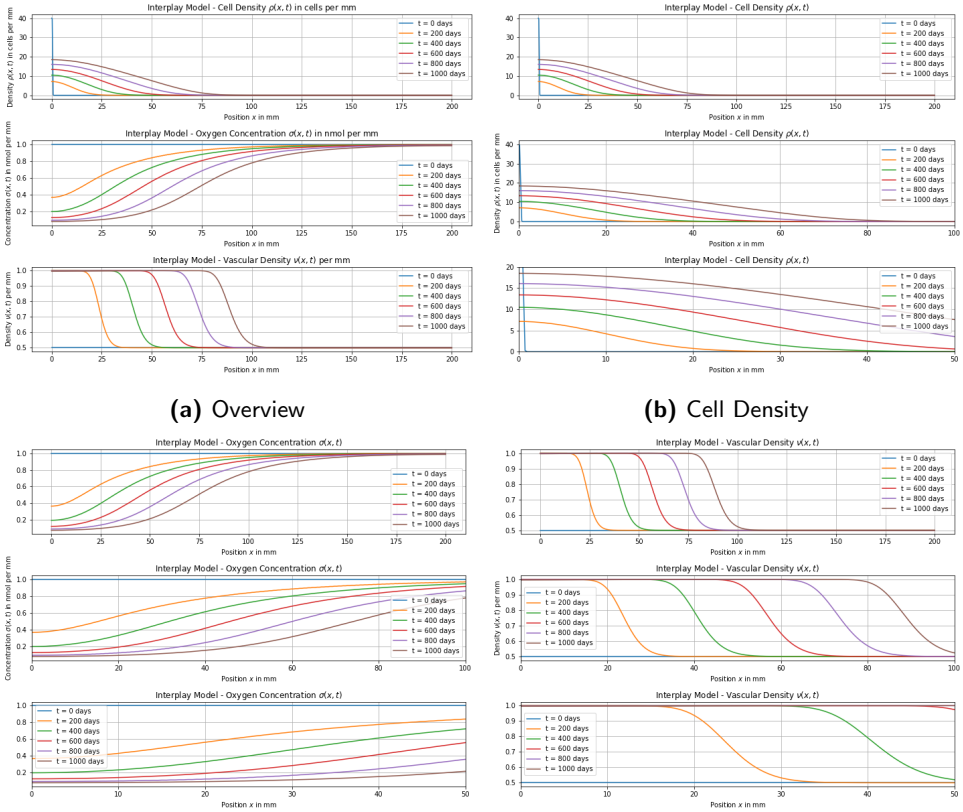

(a) Overview **(b)** Cell Density

(c) Oxygen Concentration **(d)** Vascular Density

Figure B.10: Implementation of the interplay model. The figure provides the plot for the interplay model, using the explicit scheme described in equation (4.35). The parameters are described in table 4.1. Here, we assume a diffusion rate of glioma cells of $D_\rho = 2.73 \times 10^{-1}\text{mm}^2$ per day, a proliferation rate of glioma cells of $b_\rho = 2.73 \times 10^{-2}$ per day, and an oxygen consumption rate of $h_2 = 1.14 \times 10^{-1}\text{mm}$ per cell per day. Subfigure (a) shows an overview of the model variables. Subfigures (b), (c), (d) show the cell density, oxygen concentration and the vascular density for different resolutions.

IM - Case (VI)

Here, we assume a diffusion rate of glioma cells of $D_\rho = 2.73 \times 10^{-1}\text{mm}^2$ per day, a proliferation rate of glioma cells of $b_\rho = 2.73 \times 10^{-2}$ per day, and a vaso-occlusion rate of $g_2 = 1.5 \times 10^{-11}$ cell^{-6}mm^{-6} per day. The oxygen consumption rate, h_2, stays at the baseline level.

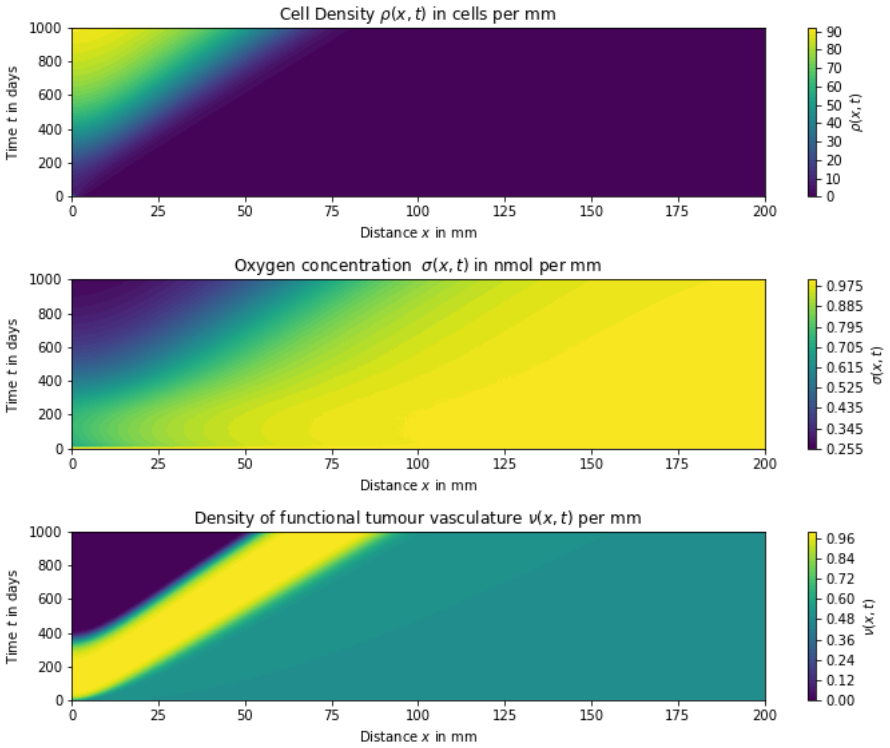

Figure B.11: Implementation of the interplay model. The figure provides the plot for the interplay model, using the explicit scheme described in equation (4.35). The parameters are described in table 4.1. Here, we assume a diffusion rate of glioma cells of $D_\rho = 2.73 \times 10^{-1}\text{mm}^2$ per day, a proliferation rate of glioma cells of $b_\rho = 2.73 \times 10^{-2}$ per day, and a vaso-occlusion rate of $g_2 = 1.5 \times 10^{-11}$ cell^{-6}mm^{-6} per day.

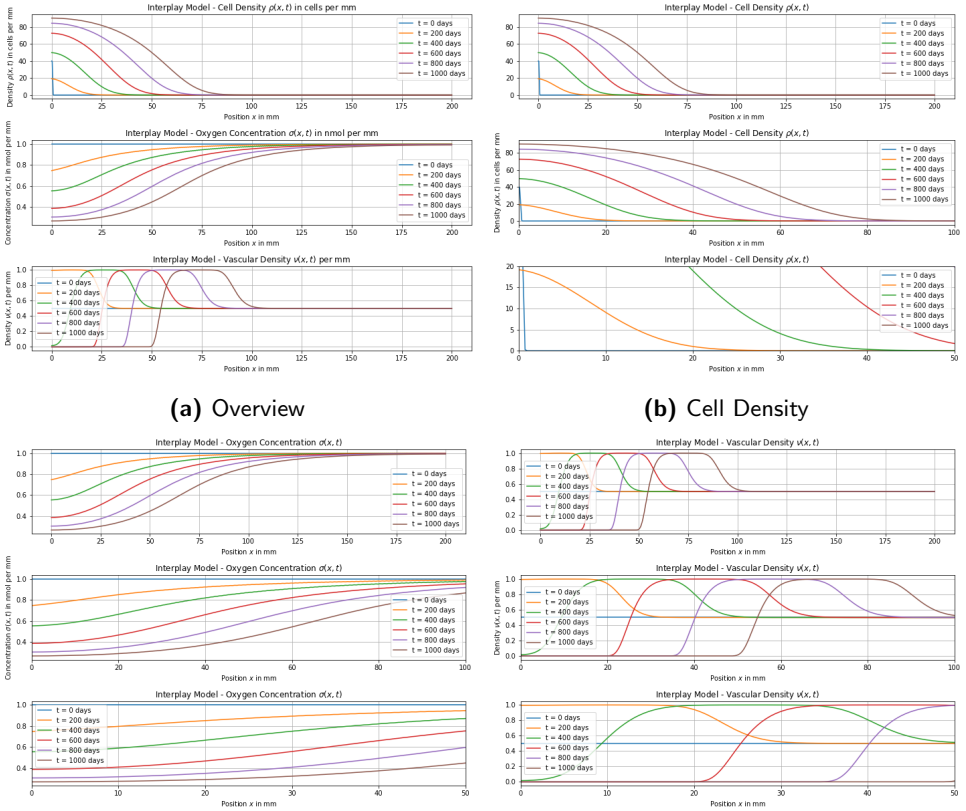

(a) Overview **(b)** Cell Density

(c) Oxygen Concentration **(d)** Vascular Density

Figure B.12: Implementation of the interplay model. The figure provides the plot for the interplay model, using the explicit scheme described in equation (4.35). The parameters are described in table 4.1. Here, we assume a diffusion rate of glioma cells of $D_\rho = 2.73 \times 10^{-1}\text{mm}^2$ per day, a proliferation rate of glioma cells of $b_\rho = 2.73 \times 10^{-2}$ per day, and a vaso-occlusion rate of $g_2 = 1.5 \times 10^{-11}$ cell^{-6}mm^{-6} per day. Subfigure (a) shows an overview of the model variables. Subfigures (b), (c), (d) show the cell density, oxygen concentration and the vascular density for different resolutions.

Appendix C

Python Code

Here we provide the python code for the Fisher-Kolmogoroff and the interplay model.

Fisher-Kolmogoroff Model - Python Code

```
#!/usr/bin/env python3
# -*- coding: utf-8 -*-
"""
Created on Fri Jun 21 21:02:50 2024

@author: JuliusSiebenaller
"""
import numpy as np
from scipy.integrate import solve_ivp
import matplotlib.pyplot as plt

# Specify the parameters and give the version a proper name:
#version = 'baseline' # Baseline version with respective parameters
#version = 'allmax' # Dp, bp at maximal values
#version = 'Dp' # Dp at max, bp at baseline
version = 'bp' # bp at max, Dp at baseline


# Parameters
# Compare Table 1 in the paper

# Parameters that changed for different cases:
Dp = 2.73e-2 # Intrinsic diffusion rate of glioma cells in mm^2 per
                                    day
    # Range: 2.73e-3 to 2.73e-1 for low- to high-grade gliomas
    # Baseline: 2.73e-2
bp = 2.73e-2 # Intrinsic proliferation rate of glioma cells
    # Range: 2.73e-4 to 2.73e-2 for low- to high-grade gliomas
    # Baseline: 2.73e-3

# Constant parameters
#Initial values for Vascular Density v0, Oxygen concentration o0,
                                    cell density p0
v0 = 0.5  # nmol per mm in the simulation domain
o0 = 1.0  # nmol per mm
p0 = 40.  # cells per mm

# Density of glioma cells: p(x,t)
BCC = 100.  # Brain carrying capacity in cells per mm (N in the
                                    model)
l1 = 2.0 # nmol per mm (Lamda_1 in the paper)
l2 = 1.0 # Lambda_2



# Define the reaction terms
def reaction_terms(p):
    p_reaction = bp * o0/l1 * p * (1-p/BCC)

    return p_reaction

# Define the system of ODEs resulting from discretization
def odes(t, y, x, Dp, dx):
    N = len(x)
    p = y[:N]
```

```
    # Compute first and second derivatives using central difference
    dp_dx = np.gradient(p, dx)
    d2p_dx2 = np.gradient(dp_dx, dx)

    # Apply Neumann boundary conditions (zero flux)
    dp_dx[0] = 0
    dp_dx[-1] = 0
    d2p_dx2[0] = d2p_dx2[1]
    d2p_dx2[-1] = d2p_dx2[-2]

    # Compute reaction terms
    p_reaction = reaction_terms(p)

    # Combine diffusion and reaction terms
    Nabla_alpha_p = (l1-o0)/l1 * d2p_dx2
    dpdt = Dp*Nabla_alpha_p + p_reaction

    return np.concatenate([dpdt])


# Initial conditions
gamma = 1.e1
eps = 0.5
def initial_conditions(x):
    p_0 = p0 * (1. - 1. / (1+ np.exp(-2.*gamma*(x-eps))))  #
                                        Initial distribution for p0
    return np.concatenate([p_0])


# Spatial domain and time span
x = np.linspace(0, 200, 1000)
t_span = (0, 1000)
dx = x[1] - x[0]
y0 = initial_conditions(x)

# Solve the system of ODEs
sol = solve_ivp(odes, t_span, y0, args=(x, Dp, dx), t_eval=np.
                                    linspace(0, 1000, 1000), method='
                                    RK45')

# Extract solutions
p_sol = sol.y[:len(x), :]
np.save('FisherSol_p' + version + '.npy', p_sol) # Save the results
                                     for the given version
    # This makes for faster plotting after initial compilation.

# Plot results
X, T = np.meshgrid(x, sol.t)

fig, ax = plt.subplots(3, 1, figsize=(10, 8))

cfp = ax[0].contourf(X, T, p_sol.T, levels=50, cmap='viridis')
fig.colorbar(cfp, ax=ax[0], label=r"\rho(x,t)")
ax[0].set_title(r"Cell Density $\rho(x,t)$ in cells per mm")
ax[0].set_xlabel("Position $x$ in mm")
ax[0].set_ylabel("Time $t$ in days")
#plt.title('Solution of Fisher-Kolmogoroff Model')
```

```
cfo = ax[1].contourf(X, T, p_sol.T, levels=50, cmap='viridis')
fig.colorbar(cfo, ax=ax[1], label=r"\rho(x,t)")
#ax[1].set_title('Solution p(x,t)')
ax[1].set_xlabel('Position $x$ in $mm$')
ax[1].set_ylabel('Time $t$ in days')
ax[1].set_xlim(0,100)
#ax[1].set_ylim(0,300)

cfv = ax[2].contourf(X, T, p_sol.T, levels=50, cmap='viridis')
fig.colorbar(cfv, ax=ax[2], label=r"\rho(x,t)")
#ax[2].set_title('Solution p(x,t)')
ax[2].set_xlabel('Position $x$ in $mm$')
ax[2].set_ylabel('Time $t$ in days')
ax[2].set_xlim(0,50)
#ax[2].set_ylim(0,150)

plt.tight_layout()
plt.savefig('FK_Model_Contour' + version + '.png')
plt.show()

# Plotting

plt.figure()
t_end = len(T)
for i in range(0, t_end, int(t_end/10)):
    #plt.plot(x, p_sol[i], label=f"t = {T[i]:.1f} days")
    plt.plot(X[i,:], p_sol[:,i], label=f"t = {i} days")
plt.plot(X[-1,:], p_sol[:,-1], label=f"t = {1000} days")
plt.title(r"Cell Density $\rho(x,t)$")
#plt.xlim(0,50)
#plt.ylim(0,40)
plt.xlabel(r"Position $x$ in mm")
plt.ylabel(r"Density $\rho(x, t)$ in cells per mm")
plt.legend()
plt.grid(True)
plt.savefig('FK_Model_Dist' + version + '.png')
plt.show()

plt.figure()
for i in range(0, t_end, int(t_end/10)):
    #plt.plot(x, p_sol[i], label=f"t = {T[i]:.1f} days")
    plt.plot(X[i,:], p_sol[:,i], label=f"t = {i} days")
plt.plot(X[-1,:], p_sol[:,-1], label=f"t = {1000} days")
plt.title(r"Cell Density $\rho(x,t)$")
plt.xlim(0,100)
#plt.ylim(0,17.50)
plt.xlabel(r"Position $x$ in mm")
plt.ylabel(r"Density $\rho(x, t)$ in cells per $mm$")
plt.legend()
plt.grid(True)
plt.savefig('FK_Model_Dist_Zoom' + version + '.png')
plt.show()

plt.figure()
for i in range(0, t_end, int(t_end/10)):
    #plt.plot(x, p_sol[i], label=f"t = {T[i]:.1f} days")
```

```
    plt.plot(X[i,:], p_sol[:,i], label=f"t = {i} days")
plt.plot(X[-1,:], p_sol[:,-1], label=f"t = {1000} days")
plt.title(r"Cell Density $\rho(x,t)$")
plt.xlim(0,50)
#plt.ylim(0,17.50)
plt.xlabel(r"Position $x$ in mm")
plt.ylabel(r"Density $\rho(x, t)$ in cells per $mm$")
plt.legend()
plt.grid(True)
plt.savefig('FK_Model_Dist_ZoomII' + version + '.png')
plt.show()

plt.figure()
for i in range(0, t_end, int(t_end/10)):
    #plt.plot(x, p_sol[i], label=f"t = {T[i]:.1f} days")
    plt.plot(X[i,:], p_sol[:,i], label=f"t = {i} days")
plt.plot(X[-1,:], p_sol[:,-1], label=f"t = {1000} days")
plt.title(r"Cell Density $\rho(x,t)$")
plt.xlim(0,25)
#plt.ylim(0,17.50)
plt.xlabel(r"Position $x$ in mm")
plt.ylabel(r"Density $\rho(x, t)$ in cells per $mm$")
plt.legend()
plt.grid(True)
plt.savefig('FK_Model_Dist_ZoomIII' + version + '.png')
plt.show()
```

Interplay Model - Python Code

```
#!/usr/bin/env python3
# -*- coding: utf-8 -*-
"""
Created on Fri Jun 21 21:02:50 2024

@author: JuliusSiebenaller
"""
import numpy as np
from scipy.integrate import solve_ivp
import matplotlib.pyplot as plt


# Specify the parameters that change and give the version a proper
                                    name:
version = 'baseline' # Baseline version with respective parameters
#version = 'allmax'         # Increase Dp, bp, h2, g2
#version = 'DiffProlifOxy'  # Increase Dp, bp, h2
#version = 'DiffProlifVaso' # Increase Dp, bp, g2
#version = 'DiffProlif'     # Increase Dp, bp
#version = 'OxyVaso'        # Increase h2, g2


# Parameters
# Compare Table 1 in the paper

# Parameters that changed for different cases:
Dp = 2.73e-2 # Intrinsic diffusion rate of glioma cells in mm^2 per
                                     day
    # Range: 2.73e-3 to 2.73e-1 for low- to high-grade gliomas
    # Baseline: 2.73e-2
bp = 2.73e-3 # Intrinsic proliferation rate of glioma cells
    # Range: 2.73e-4 to 2.73e-2 for low- to high-grade gliomas
    # Baseline: 2.73e-3
h2 = 5.73e-3 # Oxygen consumption rate in mm per cell per day
    # Range: 5.73e-3 to 1.14e-1
g2 = 5e-13 # Vaso-occlusion rate in cell^-vo_deg mm^vo_deg per day
    # Range: 5e-13 to 1.5e-11

# Constant parameters
#Initial values for Vascular Density v0, Oxygen concentration o0,
                                     cell density p0
v0 = 0.5  # nmol per mm in the simulation domain
o0 = 1.0  # nmol per mm
p0 = 40.  # cells per mm

# Density of glioma cells: p(x,t)
BCC = 100.  # Brain carrying capacity in cells per mm (N in the
                                     model)
l1 = 2.0 # nmol per mm (Lamda_1 in the paper)
l2 = 1.0 # Lambda_2

# Oxygen concentration: o(x,t)
Do = 1.51e2  # Oxygen diffusion rate in mm^2 per day
h1 = 3.37e-1  # Oxygen supply rate per day

# Vasculature density: v(x,t)
```

```
Dv = 5.0e-4 # mm^2 per day - Vasculature dispersal rate
g1 = 0.1  # Vasculature formation rate - per day
oa_star = 2.5e-1  # Oxygen concentration threshold for hypoxia -
                                    nmol per mm
K = 1.0  # Half maximal pro-angiogenic factor concentration  -nmol
                                    per mm
vo_deg = 6.  # Dimensionless vaso-occlusion degree
theta = 10.  # Heaviside parameter vasculature



# Define the reaction terms
def reaction_terms(p, o, v):
    p_reaction = bp * o / l1 * p * (1 - p / BCC)
    o_star_diff = o - oa_star
    v_reaction = g1 * p * np.heaviside(o_star_diff,0) * (1 - v) / (
                                        K + p * np.heaviside(
                                        o_star_diff,0) / v) - g2 * v
                                        * p ** vo_deg
    o_reaction = h1 * v0 * (o0 - o) - h2 * p * o

    return p_reaction, o_reaction, v_reaction


# Define the system of ODEs resulting from discretization
def odes(t, y, x, Dp, Do, Dv, dx):
    N = len(x) # solutions are stored in a 1-dim array
    p = y[:N]
    o = y[N:2*N]
    v = y[2*N:]

    # Compute first and second derivatives using central difference
    dp_dx = np.gradient(p, dx)
    do_dx = np.gradient(o, dx)
    dv_dx = np.gradient(v, dx)
    d2p_dx2 = np.gradient(dp_dx, dx)
    d2o_dx2 = np.gradient(do_dx, dx)
    d2v_dx2 = np.gradient(dv_dx, dx)

    # Apply Neumann boundary conditions (zero flux)
    dp_dx[0] = 0
    dp_dx[-1] = 0
    do_dx[0] = 0
    do_dx[-1] = 0
    dv_dx[0] = 0
    dv_dx[-1] = 0
    # And smoothness at the boundaries
    d2p_dx2[0] = d2p_dx2[1]
    d2p_dx2[-1] = d2p_dx2[-2]
    d2o_dx2[0] = d2o_dx2[1]
    d2o_dx2[-1] = d2o_dx2[-2]
    d2v_dx2[0] = d2v_dx2[1]
    d2v_dx2[-1] = d2v_dx2[-2]

    # Compute reaction terms
    p_reaction, o_reaction, v_reaction = reaction_terms(p, o, v)
```

```
    # Combine diffusion and reaction terms
    Nabla_alpha_p = (l1*d2p_dx2 - 2.*dp_dx*do_dx - o*d2p_dx2 -
                                    d2o_dx2*p) / l1
    dpdt = Dp*Nabla_alpha_p + p_reaction
    dvdt = Dv * d2v_dx2 + v_reaction
    dodt = Do * d2o_dx2 + o_reaction

    return np.concatenate([dpdt, dodt, dvdt])


# Initial conditions
gamma = 1.e1
eps = 0.5
def initial_conditions(x):
    # Here, we follow the model and provide a smooth initial
                                    distribution of the tumour
                                    cell density
    p_0 = p0 * (1. - 1. / (1+ np.exp(-2.*gamma*(x-eps))))  #
                                    Initial distribution for p
    o_0 = o0 * np.ones_like(x) # Initial condition for oxygen
                                    concentration
    v_0 = v0 * np.ones_like(x) # Initial condition for functional
                                    vasculature
    return np.concatenate([p_0, o_0, v_0])

# Spatial domain and time span
x = np.linspace(0, 200, 800) # 200mm divided in 800 points
t_span = (0, 1000) # model for close to 3 years
dx = x[1] - x[0]
y0 = initial_conditions(x)

# Solve the system of ODEs
sol = solve_ivp(odes, t_span, y0, args=(x, Dp, Do, Dv, dx), t_eval=
                                    np.linspace(0, 1000, 80), method=
                                    'RK45')

# Extract solutions
p_sol = sol.y[:len(x), :]
o_sol = sol.y[len(x):2*len(x), :]
v_sol = sol.y[2*len(x):, :]
# Save the results for the given version. This allows for faster
                                    plotting after initial
                                    compilation.
np.save('ModelIII_p' + version + '.npy', p_sol)
np.save('ModelIII_o' + version + '.npy', o_sol)
np.save('ModelIII_v' + version + '.npy', v_sol)


# Plot results
X, T = np.meshgrid(x, sol.t)
np.save('ModelIII_X' + version + '.npy', X) # Position vector
np.save('ModelIII_T' + version + '.npy', T) # Time vector


# Use a contourplot for a first overview.
fig, ax = plt.subplots(3, 1, figsize=(10, 8))
```

```
cfp = ax[0].contourf(X, T, p_sol.T, levels=50, cmap='viridis')
fig.colorbar(cfp, ax=ax[0], label=r"$\rho(x,t)$")
ax[0].set_title(r"Cell Density $\rho (x,t)$ in cells per mm")
ax[0].set_xlabel(r"Distance $x$ in mm")
ax[0].set_ylabel(r"Time $t$ in days")

cfo = ax[1].contourf(X, T, o_sol.T, levels=50, cmap='viridis')
fig.colorbar(cfo, ax=ax[1], label=r"$\sigma(x,t)$")
ax[1].set_title(r"Oxygen concentration  $\sigma (x,t)$ in nmol per
                                    mm")
ax[1].set_xlabel(r"Distance $x$ in mm")
ax[1].set_ylabel(r"Time $t$ in days")

cfv = ax[2].contourf(X, T, v_sol.T, levels=50, cmap='viridis')
fig.colorbar(cfv, ax=ax[2], label=r"$\nu(x,t)$")
ax[2].set_title(r"Density of functional tumour vasculature $\nu(x,t
                                    )$ per mm")
ax[2].set_xlabel(r"Distance $x$ in mm")
ax[2].set_ylabel(r"Time $t$ in days")

plt.tight_layout()
#plt.savefig('Model_III_Overview.png')
plt.savefig('Model_III_Overview_' + version + '.png')
plt.show()

# Plot zoomed-in version
plt.figure()
#plt.figure(figsize=(10, 6))
for i in range(0, 80, 8):
    #plt.plot(x, p_sol[i], label=f"t = {T[i]:.1f} days")
    plt.plot(X[-1,:], p_sol.T[i,:], label=f"t = {i*1000/80:.1f}
                                        days")
plt.plot(X[-1,:], p_sol.T[-1,:], label=f"t = {1000:.0f} days")
plt.title(r"Interplay Model - Cell Density $\rho(x,t)$")
#plt.xlim(0,10)
#plt.ylim(0,40)
plt.xlabel(r"Position $x$ in mm")
plt.ylabel(r"Density $\rho(x, t)$ in cells per mm")
plt.legend()
plt.grid(True)
plt.savefig('Model_III_CellDens_' + version + '.png')
plt.show()


plt.figure()
#plt.figure(figsize=(10, 6))
for i in range(0, 80, 8):
    plt.plot(X[-1,:], o_sol.T[i,:], label=f"t = {i*1000/80:.0f}
                                        days")
plt.plot(X[-1,:], o_sol.T[-1,:], label=f"t = {1000:.0f} days")
plt.title("Interplay Model - Oxygen Concentration $\sigma(x,t)$")
#plt.xlim(0,30)
#plt.ylim(0,40)
plt.xlabel("Position $x$ in mm")
plt.ylabel("Density $\sigma(x, t)$ in nmol per mm")
plt.legend()
plt.grid(True)
```

```
plt.savefig('Model_III_OxConc_' + version + '.png')
plt.show()

plt.figure()
#plt.figure(figsize=(10, 6))
for i in range(0, 80,8):
    plt.plot(X[-1,:], v_sol.T[i,:], label=f"t = {i*1000/80:.0f}
                                        days")
    #print(i)
plt.plot(X[-1,:], v_sol.T[-1,:], label=f"t = {1000:.0f} days")
plt.title(r"Interplay Model - Vasculature Density $\nu(x,t)$")
#plt.xlim(0,30)
#plt.ylim(0,40)
plt.xlabel(r"Position $x$ in mm")
plt.ylabel(r"Density $\nu(x, t)$ per mm")
plt.legend()
plt.grid(True)
plt.savefig('Model_III_VascDens_' + version + '.png')
plt.show()


# Creating Multiple Subplots for Line Plots
fig, axes = plt.subplots(3, 1, figsize=(10, 8))
# Line Plot 1
for i in range(0, 80, 16):
    axes[0].plot(X[-1,:], p_sol.T[i,:], label=f"t = {i*1000/80:.0f}
                                        days")
axes[0].plot(X[-1,:], p_sol.T[-1,:], label=f"t = {1000:.0f} days")
axes[0].set_title(r"Interplay Model - Cell Density $\rho(x,t)$ in
                                    cells per mm")
#axes[0].set_xlim(0,20)
axes[0].set_xlabel(r"Position $x$ in mm")
axes[0].set_ylabel(r"Density $\rho(x,t) $ in cells per mm")
axes[0].grid()
axes[0].legend()

for i in range(0, 80, 16):
    axes[1].plot(X[-1,:], o_sol.T[i,:], label=f"t = {i*1000/80:.0f}
                                        days")
axes[1].plot(X[-1,:], o_sol.T[-1,:], label=f"t = {1000:.0f} days")
axes[1].set_title(r"Interplay Model - Oxygen Concentration $\sigma(
                                    x,t)$ in nmol per mm")
#axes[1].set_xlim(0,30)
axes[1].set_xlabel("Position $x$ in mm")
axes[1].set_ylabel("Concentration $\sigma(x, t)$ in nmol per mm")
axes[1].grid()
axes[1].legend()

for i in range(0, 80, 16):
    axes[2].plot(X[-1,:], v_sol.T[i,:], label=f"t = {i*1000/80:.0f}
                                        days")
axes[2].plot(X[-1,:], v_sol.T[-1,:], label=f"t = {1000:.0f} days")
axes[2].set_title(r"Interplay Model - Vascular Density $\nu(x,t)$
                                    per mm")
#axes[2].set_xlim(0,50)
axes[2].set_xlabel(r"Position $x$ in mm")
axes[2].set_ylabel(r"Density $\nu(x, t)$ per mm")
```

```
axes[2].grid()
axes[2].legend()

# Adjusting layout
plt.tight_layout()

# Show the plots
plt.savefig('Model_III_Overview_Line_' + version + '.png')
plt.show()

# Creating Multiple Subplots for Line Plots - Cell Density
fig, axes = plt.subplots(3, 1, figsize=(10, 8))
# Line Plot 1
for i in range(0, 80, 16):
    axes[0].plot(X[-1,:], p_sol.T[i,:], label=f"t = {i*1000/80:.0f}
                                        days")
axes[0].plot(X[-1,:], p_sol.T[-1,:], label=f"t = {1000:.0f} days")
axes[0].set_title(r"Interplay Model - Cell Density $\rho(x,t)$")
#axes[0].set_xlim(0,20)
axes[0].set_xlabel(r"Position $x$ in mm")
#axes[0].set_ylabel(r"Density $\rho(x, t)$ in cells per mm")
axes[0].grid()
axes[0].legend()

for i in range(0, 80, 16):
    axes[1].plot(X[-1,:], p_sol.T[i,:], label=f"t = {i*1000/80:.0f}
                                        days")
axes[1].plot(X[-1,:], p_sol.T[-1,:], label=f"t = {1000:.0f} days")
axes[1].set_title(r"Interplay Model - Cell Density $\rho(x,t)$")
axes[1].set_xlim(0,100)
axes[1].set_xlabel(r"Position $x$ in mm")
axes[1].set_ylabel(r"Density $\rho(x, t)$ in cells per mm")
axes[1].grid()
axes[1].legend()

for i in range(0, 80, 16):
    axes[2].plot(X[-1,:], p_sol.T[i,:], label=f"t = {i*1000/80:.0f}
                                        days")
axes[2].plot(X[-1,:], p_sol.T[-1,:], label=f"t = {1000:.0f} days")
axes[2].set_title(r"Interplay Model - Cell Density $\rho(x,t)$")
axes[2].set_xlim(0,50)
axes[2].set_ylim(0,20)
axes[2].set_xlabel(r"Position $x$ in mm")
#axes[2].set_ylabel(r"Density $\rho (x,t)$ in cells per mm")
axes[2].grid()
axes[2].legend()

# Adjusting layout
plt.tight_layout()

# Show the plots
plt.savefig('Model_III_Overview_Cell_Line_' + version + '.png')
plt.show()

# Creating Multiple Subplots for Line Plots - Oxygen Concentration
fig, axes = plt.subplots(3, 1, figsize=(10, 8))
# Line Plot 1
```

```
for i in range(0, 80, 16):
    axes[0].plot(X[-1,:], o_sol.T[i,:], label=f"t = {i*1000/80:.0f}
                                        days")
axes[0].plot(X[-1,:], o_sol.T[-1,:], label=f"t = {1000:.0f} days")
axes[0].set_title(r"Interplay Model - Oxygen Concentration $\sigma(
                                    x,t)$")
#axes[0].set_xlim(0,20)
axes[0].set_xlabel(r"Position $x$ in mm")
#axes[0].set_ylabel(r"Concentration $\sigma(x, t)$ in nmol per mm")
axes[0].grid()
axes[0].legend()

for i in range(0, 80, 16):
    axes[1].plot(X[-1,:], o_sol.T[i,:], label=f"t = {i*1000/80:.0f}
                                        days")
axes[1].plot(X[-1,:], o_sol.T[-1,:], label=f"t = {1000:.0f} days")
axes[1].set_title(r"Interplay Model - Oxygen Concentration $\sigma(
                                    x,t)$")
axes[1].set_xlim(0,100)
axes[1].set_xlabel(r"Position $x$ in mm")
axes[1].set_ylabel(r"Concentration $\sigma(x, t)$ in nmol per mm")
axes[1].grid()
axes[1].legend()

for i in range(0, 80, 16):
    axes[2].plot(X[-1,:], o_sol.T[i,:], label=f"t = {i*1000/80:.0f}
                                        days")
axes[2].plot(X[-1,:], o_sol.T[-1,:], label=f"t = {1000:.0f} days")
axes[2].set_title(r"Interplay Model - Oxygen Concentration $\sigma(
                                    x,t)$")
axes[2].set_xlim(0,50)
#axes[2].set_ylim(0,15)
axes[2].set_xlabel(r"Position $x$ in mm")
#axes[2].set_ylabel(r"Concentration $\sigma(x, t)$ in nmol per mm")
axes[2].grid()
axes[2].legend()

# Adjusting layout
plt.tight_layout()

# Show the plots
plt.savefig('Model_III_Overview_Oxy_Line_' + version + '.png')
plt.show()


# Creating Multiple Subplots for Line Plots - Vascular Density
fig, axes = plt.subplots(3, 1, figsize=(10, 8))
# Line Plot 1
for i in range(0, 80, 16):
    axes[0].plot(X[-1,:], v_sol.T[i,:], label=f"t = {i*1000/80:.0f}
                                        days")
axes[0].plot(X[-1,:], v_sol.T[-1,:], label=f"t = {1000:.0f} days")
axes[0].set_title(r"Interplay Model - Vascular Density $\nu(x,t)$")
#axes[0].set_xlim(0,20)
axes[0].set_xlabel(r"Position $x$ in mm")
#axes[0].set_ylabel(r"Density $\nu(x, t)$ per mm")
axes[0].grid()
```

```
axes[0].legend()

for i in range(0, 80, 16):
    axes[1].plot(X[-1,:], v_sol.T[i,:], label=f"t = {i*1000/80:.0f}
                                        days")
axes[1].plot(X[-1,:], v_sol.T[-1,:], label=f"t = {1000:.0f} days")
axes[1].set_title(r"Interplay Model - Vascular Density $\nu(x,t)$")
axes[1].set_xlim(0,100)
axes[1].set_xlabel(r"Position $x$ in mm")
axes[1].set_ylabel(r"Density $\nu(x, t)$ per mm")
axes[1].grid()
axes[1].legend()

for i in range(0, 80, 16):
    axes[2].plot(X[-1,:], v_sol.T[i,:], label=f"t = {i*1000/80:.0f}
                                        days")
axes[2].plot(X[-1,:], v_sol.T[-1,:], label=f"t = {1000:.0f} days")
axes[2].set_title(r"Interplay Model - Vascular Density $\nu(x,t)$")
axes[2].set_xlim(0,50)
#axes[2].set_ylim(0,15)
axes[2].set_xlabel(r"Position $x$ in mm")
#axes[2].set_ylabel(r"Density $\nu(x, t)$ per mm")
axes[2].grid()
axes[2].legend()

# Adjusting layout
plt.tight_layout()

# Show the plots
plt.savefig('Model_III_Overview_Vasc_Line_' + version + '.png')
plt.show()
```

Appendix D

Declaration of originality

Attached is the declaration of originality.

In accordance with the Declaration of originality, I state that I have used generative artificial intelligence technologies for revising this thesis with regards to spelling and grammar mistakes and conversion to British English. For this, I relied on ChatGPT (GPT-4) from OpenAI [45].

ETH

Eidgenössische Technische Hochschule Zürich
Swiss Federal Institute of Technology Zurich

Declaration of originality

The signed declaration of originality is a component of every written paper or thesis authored during the course of studies. In consultation with the supervisor, one of the following three options must be selected:

○ I confirm that I authored the work in question independently and in my own words, i.e. that no one helped me to author it. Suggestions from the supervisor regarding language and content are excepted. I used no generative artificial intelligence technologies[1].

⊗ I confirm that I authored the work in question independently and in my own words, i.e. that no one helped me to author it. Suggestions from the supervisor regarding language and content are excepted. I used and cited generative artificial intelligence technologies[2].

○ I confirm that I authored the work in question independently and in my own words, i.e. that no one helped me to author it. Suggestions from the supervisor regarding language and content are excepted. I used generative artificial intelligence technologies[3]. In consultation with the supervisor, I did not cite them.

Title of paper or thesis:

Reaction-diffusion models in the context of brain tumours

Authored by:
If the work was compiled in a group, the names of all authors are required.

Last name(s):	**First name(s):**
Siebenaller	Julius

With my signature I confirm the following:
- I have adhered to the rules set out in the Citation Guide.
- I have documented all methods, data and processes truthfully and fully.
- I have mentioned all persons who were significant facilitators of the work.

I am aware that the work may be screened electronically for originality.

Place, date	**Signature(s)**
Zürich, 25.06.2024	

If the work was compiled in a group, the names of all authors are required. Through their signatures they vouch jointly for the entire content of the written work.

[1] E.g. ChatGPT, DALL E 2, Google Bard
[2] E.g. ChatGPT, DALL E 2, Google Bard
[3] E.g. ChatGPT, DALL E 2, Google Bard